UNIVERSITÀ DEGLI STUDI DELL'INSUBRIA

PhD School of Biological and Medical Sciences

PhD Program in Experimental and Clinical Physiology

XXVIII CICLO

Functional characterization of iron transporters Nramp1 and Nramp2 from *Dictyostelium discoideum*: a model of cellular iron homeostasis

Tutors: Prof. Daniela Negrini, Prof. Elena Bossi
Coordinator: Prof. Daniela Negrini

PhD Student Dott. Francesca Guia Imperiali

ANNO ACCADEMICO 2016/2017

A Filippo e Carlotta

gli esperimenti migliori della mia vita

Index

Research activity of the PhD program has been reported in the following manuscript:

Buracco S, Peracino B, Cinquetti R, Signoretto E, Vollero A, **Imperiali FG**, Castagna M, Bossi E, Bozzaro S. **Dictyostelium Nramp1, which is structurally and functionally similar to mammalian DMT1 transporter, mediates phagosomal iron efflux.** J Cell Sci. 2015 Sep 1;128(17):3304-16. doi: 10.1242/jcs.173153.

Part of my research also focused on other membrane transporters:

Margheritis E*, **Imperiali FG***, Cinquetti R, Vollero A, Terova G, Rimoldi S, Girardello R, Bossi E. **Amino acid transporter B(0)AT1 (slc6a19) and ancillary protein: impact on function.** Pflugers Arch. 2016 Aug;468(8):1363-74. doi: 10.1007/s00424-016-1842-5.

*Margheritis and Imperiali contributed equally to this work.

Vollero A*, **Imperiali FG***, Cinquetti R, Margheritis E, Peres A, Bossi E. **The D-amino acid transport by the invertebrate SLC6 transporters KAAT1 and CAATCH1 from Manduca sexta.** Physiol Rep. 2016 Feb;4(4). pii: e12691. doi: 10.14814/phy2.12691.

*Vollero and Imperiali contributed equally to this work.

And in the following abstract presented in scientific meetings:

9th SFB35–Symposium: "TRANSMEMBRANE TRANSPORTERS IN HEALTH AND DISEASE" - Institute of Pharmacology-Vienna August 31-September 2, 2016. **Measuring of transport activity in Xenopus laevis oocytes by fluorophore quencing. Imperiali FG**, Cinquetti R, Zanella D, Mihatovic S, Peracino B, Bozzaro S, Bossi E. Abstract and Poster presentation.

8th SFB35–Symposium: "TRANSMEMBRANE TRANSPORTERS IN HEALTH AND DISEASE" - Institute of Pharmacology-Vienna September 7-9, 2015. **The invertebrate SLC6 transporters KAAT1 and CAATCH1 from Manduca sexta are able to transport D-amino acid.** Bossi E. Vollero A,**Imperiali FG**, Zanella D, Cinquetti R.

7th SFB35–Symposium: "TRANSMEMBRANE TRANSPORTERS IN HEALTH AND DISEASE" - Institute of Pharmacology-Vienna September 8-10, 2014. **Functional characterization of Dyctiostelium Nramp1 and Nramp2, which confer resistance to bacterial infection and are essential for iron transport.** Cinquetti R, Peracino B, **Imperiali FG**, Vollero A, Zanella D, Castagna M, Buracco S, Bozzaro S, Bossi E. Abstract and Poster presentation.

6th SFB35–Symposium: "TRANSMEMBRANE TRANSPORTERS IN HEALTH AND DISEASE" - Institute of Pharmacology-Vienna September 23-25, 2013.

Residues involved in transport mechanism in the amino acid transporter KAAT1 (SLC6 family). Bossi E, Giovanola M, Vollero A, **Imperiali FG**, Sacchi VF, Castagna M. Abstract and Poster presentation.

INTRODUCTION

CHAPTER 1
IRON

IRON HOMEOSTASIS

Iron is an element necessary for all the organisms for life; its role in essential metabolism, cellular processes, energy production, biosynthesis is well described. Although being so important, it has damaging properties in its free form. Its capacity to change between the +2 and +3 oxidation states, may produce reactive oxygen species (ROS) responsible for cellular and tissue damage. In order to neutralize those negative effects iron need to be associated with proteins: in the plasma is mainly coupled with transferrin; in the cell is linked to chaperones or storage within ferritin. In mammals, heme synthesis during erythropoiesis requires the highest amount of iron; erythrocytes, fundamental for their role in respiration, are mostly constituted of haemoglobin (4 heme group/Hb), erythrophagocytosis, mediated by macrophages, remove senescent erythrocytes from circulation and makes iron newly reusable. Iron homeostasis is finely regulated at different level and with different protagonists: enterocytes absorb iron from food, macrophages recycle iron derived from erythrocytes destruction, hepatocytes are the principal storage of iron. Hepcidin, a liver hormone, plays a key role in the process; its transcription is up-regulated by high iron levels, infection and inflammation, on the other hand down regulated by anemia and erythropoiesis. Hepcidin binds the iron exporter (unique in all the cells and organisms) ferroportin-1 (Fpn1) at the cell surface causing its internalization and degradation. Moreover the iron homeostasis is localized also at cellular level to regulate the expression of genes related to iron metabolism. Iron regulatory protein (IRP)/iron responsive element (IRE) system controls both mRNA stability and translation of proteins involved in iron homeostasis [1].

HUMAN IRON METABOLISM

In the human body iron is present as ferrous (Fe^{2+}) and ferric (Fe^{3+}) iron [2]. Fe^{3+} is the most stable ion with physiological concentration of oxygen. Fe^{2+} reduces O_2 with the formation of superoxide radicals [3]. The presence of ROS is responsible for damaging

proteins, nucleic acids and carbohydrates, and for starting lipid peroxidation and, lastly, cellular apoptosis [4]. Thus, is important for iron metabolism prevent the formation of free iron. All mechanisms, involved in this process, comprehend iron absorption in the gut, transport via circulation, cellular intake and utilization, macrophagic recycle and liver storage [5,6] (Figure 1).

Absorption

Iron derived from food is heme iron or non-heme iron [7]; the first is present in meat as haemoglobin and myoglobin. Heme release from hemo proteins is due to the low pH of the stomach combined to proteolytic enzymes. Heme uptake in enterocyte is mediated by the heme-carrier protein 1 (HCP1), together with the proton coupled folate transporter (PCFT) (Figure 1A); the latter has low-affinity to heme and is more involved in folate absorption [8]. Inside the cell heme oxygenase 1 (HO1) breaks heme and release Fe^{3+}. Non-heme iron is mainly Fe^{3+}; acid pH of the stomach and ascorbic acid reduce Fe^{3+} to Fe^{2+} to permit the uptake in the enterocyte [7]. Apical membrane of enterocyte presents on its surface all the proteins necessary for iron absorption. In particular proteins for iron reduction, such as duodenal cytochrome b (DcytB) and six transmembrane epithelial antigen of the prostate 2 (Steap2) [9,10], and for iron uptake in the cell, the proton-coupled divalent metal transporter 1 (DMT1) (Figure 1A). DMT1 is involved in the absorption of different divalent metal ions (iron, cobalt, manganese, zinc, cadmium and others); it is a transmembrane protein that perform the symport of Fe^{2+} coupled with H^{+} , utilizing the proton gradient between the gut lumen and the enterocyte cytoplasm [11]. Inside the cell iron is addressed to the basolateral membrane to be exported or stored in ferritin. It is notable that, in mice, the absence of the IRE/IRP system increases ferritin levels, iron is blocked in the enterocyte, independently of the iron status of the organism [12]. The access of iron in the whole body with circulation depend on the export of iron from the enterocyte; Fpn1 is expressed at basolateral membrane of enterocyte, is the only mammal iron exporter [13]; Fpn1 transports Fe^{2+} outside the basolateral membrane where ferroxidases, hephaestin (Heph) and ceruloplasmin (Cp) oxidize Fe^{2+} to Fe^{3+} to be associated with transferrin (Tf) in circulation [14,15] (Figure 1A).

Transport and cellular uptake

After absorption iron is distributed in the organism conjugated with transferrin. The oxidation state, the protein conformation and pH influence the stability of transferrin-bound iron (TBI). Tf could be found in the plasma in three different forms: apo-transferrin (apo-Tf), protein without iron; monoferric transferrin (with a single iron atom); and diferric transferrin or holotransferrin (holo-Tf; with two iron atoms) [16]. The acute need of iron is regulated with the presence of these three states of Tf avoiding the negative effects of iron excess in the organism. Transferrin receptor1 (TfR1), located in cell membrane, is responsible for cellular uptake of TBI [17]. Next step is a clathrin-dependent endocytosis of the TBI–TfR1 complex. The intake of H^+ by an ATP-dependent proton pump acidifies the endosome causing the release of Fe^{3+}, while apo-Tf remains complexed with TfR1. In the endosome, Fe^{3+} is converted by Steap 3 to $Fe^{2+}$and transported by DMT1 in the cytoplasm [11,18]. At the same time, the Tf–TfR1 complex return to the cell membrane where apo-Tf return in the circulation (Figure 1B). Exists also a non-transferrin bound iron (NTBI) form detected in the plasma [19]. Mainly NTBI is Fe^{3+} bound to citrate or acetate [20]; this different iron is mainly directed to hepatocytes where the zinc transporter Zrt–Irt-like protein 14 (Zip 14) [21] mediates the uptake with an endocytosis-independent mechanism.

Consumption and storage

Synthesis of haemoglobin in the erythroblasts is the principal cause of high iron necessity. Heme iron in erythrocytes corresponds to 70% of the body iron pool [22]. Iron released from endosome is conducted to mitochondrion, the principal organelle responsible for cellular iron homeostasis. Iron is driven to mitochondria by a cytosolic iron chaperon, the poly (rC) binding protein 1 (PCBP1) [23], or directly from the endosome with a ‘kiss-and-run’ mechanism (seen in immature erythrocyte where haemoglobin synthesis is higher) [24]; in mitochondria iron is fundamental for biosynthesis of heme. Beyond iron utilization in biosynthesis, iron storage is also important to avoid the presence of free iron or to provide rapid accessibility during iron deficiency. Principal contributor in iron storage is the ferritin (Ft) protein [25] (Figure 1C). Ferritin is a 24-subunit multimer of heavy (Ft-H) and light (Ft-L) polypeptide chains; after synthesis, these chains self-assemble in a spherical structure that is able to

incorporate up to 4500 iron atoms inside. PCBP chaperones drive cytosolic Fe^{2+} to Ft, Ft-H subunit oxidizes Fe^{2+} to Fe^{3+}, Ft-L subunit is responsible for its uptake into the core [23]. Ft is in the cytosol, nucleus and mitochondria, but is also present in the serum (sFt). Mitochondria present their own Ft-H-like chains; in particular, the mitochondrial Ft (mFt) is more efficient than the cytoplasmic one to store iron [26]. The iron release from Ft is mediated by lysosome and proteasome degradation [27,28]. The nuclear receptor coactivator 4 (NCOA4) is a cargo receptor that binds and carry Ft in lysosomes, regulating iron bioavailability [29]. Accordingly, NCOA4 expression is up-regulated during erythropoiesis-a process with high necessity of iron-[30]. Ncoa4−/− mice showed a severe iron overload in splenic macrophages-responsible of iron recycle in senescent erythrocytes- suggesting the importance of NCOA4 in iron *equilibrium* [31].

Recycling

Splenic and hepatic macrophages scavenges senescent erythrocytes to obtain iron from haemoglobin ready to be reutilized in the synthesis of new molecules of haemoglobin [32] (Figure 1D). Macrophages are able to detect markers of aging on erythrocyte membranes [33-36]; in particular: alteration in the erythrocyte solute carrier family 4 (anion exchanger) member 1 (SLC4A1), the presence of membrane phosphatidylserine, and the decrease of membrane flexibility, sialic acid and in CD47 antigen. All these modifications elicit erythrocyte phagocytosis macrophage mediated; in the phagolysosome, ROS and hydrolytic enzymes cause the release of heme from erythrocyte to the vacuolar fluid. Then, HO1 together with O_2 split heme in iron, CO and biliverdin [37]. Intravascular hemolysis causes the release of haemoglobin in circulation, where it is conjugated with haptoglobin; this protein is recognized by CD163, membrane macrophage receptor [38] (Figure 1D). The transport of iron within the macrophage comprehend: (a) phagosome membrane transport mediated by DMT1 transporter and the natural resistance-associated macrophage protein (Nramp1) [39]; (b) movement in the cytoplasm with PCBP chaperones [31]; and (c) Fpn1 for the release of Fe^{2+} outside the cell where the enzyme glycosylphosphatidylinositol-linked (Gpi)-ceruloplasmin oxidizes Fe^{2+} to Fe^{3+} and allows the binding of Fe^{3+} to serum Tf [40].

REGULATION OF IRON METABOLISM

Iron homeostasis in human organism is committed to several mechanisms: control of iron absorption, recycling and storage. Given that there are no mechanisms for iron excretion, only 1 mg of dietary iron every day is needed. This process exceeds the non specific iron losses caused by bleeding, sweat and sloughing of epithelial cells. The increased need of iron involves augmented duodenal absorption and release from macrophages and from storage cells (mainly epatocytes). On the other hand, iron overload induces the inhibition of absorption and increases storage, to avoid toxic effects of excessive free iron [41,42]. Iron homeostasis is finely regulated at systemic and cellular level.

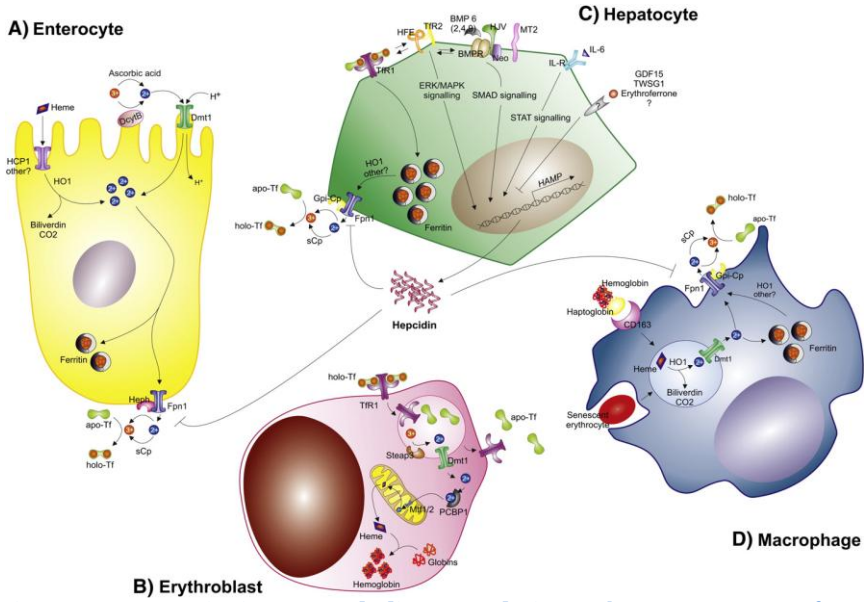

Figure 1. Systemic iron metabolism regulation. The maintenance of iron homeostasis includes the regulation of (A) dietary iron by duodenum enterocyte, (B) usage by erythroblasts, (C) storage by hepatocytes and (D) recycling by splenic macrophages. After being reduced by ascorbic acid and Dcytb at the apical membrane of enterocytes, iron is absorbed by DMT1 and driven to the basolateral membrane of these cells where it is exported by Fpn1 to circulation associated with transferrin (holo-Tf). Erythrocytes, which require the major amounts of iron, capture holo-Tf through the membrane-associated TfR1. After being endocytosed, iron is used by mitochondria for heme synthesis. If iron absorbed is more than required, it is stored in ferritin, mostly in hepatocytes. The most common source of iron are macrophages, as they phagocyte the senescent erythrocytes, releasing iron from heme through the HO1, rendering it available to be reutilized by the cells. In the control of all of these processes there is hepcidin, a circulatory protein synthesized in the liver accordingly to iron levels. Hepcidin acts by binding membrane-associated Fpn1, inducing its internalization and degradation and, consequently, preventing dietary iron absorption and release from storing hepatocytes and recycling macrophages. Modified from [1].

Systemic regulation

The principal regulator of iron homeostasis is hepcidin, it is a hormone peptide of 25 amino acid mainly synthesized in the liver [43]. Many physiological conditions play a role in hepcidin expression: systemic iron levels, hypoxia, anemia, erythropoiesis, infection and inflammation [44-46] (Figure 1C). HAMP gene on chromosome 19 encodes for hepcidin protein. The synthesis starts with an inactive pre-pro-protein of 84 aa-with signal peptide, pro-region and the active sequence of 25 aa [47]. In cell hepcidin becomes mature via a proteolytic cleavage due to the prohormone convertase furin [48]. Hepcidin promotes Fpn1 internalization and, consequent degradation [49] (Figure 1). The mechanism of internalization involves a rapid ubiquitination of Fpn1 [50]. Thank to this mechanism, hepcidin controls dietary iron uptake and release from macrophages, hepatocytes and other cells involved in systemic iron metabolism. HAMP expression is induced by iron overload, infection and inflammation [44,49,51], whereas reduced by iron deficiency, hypoxia, anemia and erythropoiesis [45,46] (Figure 2).

Iron levels

Iron level permits the regulation of HAMP expression, avoiding toxic effects of iron overload or negative consequences of iron deficiency. Hepatocytes showed different proteins on its membranes named “iron sensors”: hemojuvelin (Hjv), HFE, TfR1, and TfR2 [1]. Hjv-bone morphogenetic protein (BMP) axis controls HAMP expression principally in the liver [54]. Hjv is the co-receptor of BMPs-cytokines belonging to the transforming growth factor β superfamily [55]. The binding of BMP to Hjv and BMP activates phosphorylation of cytosolic SMADs 1, 5 and 8 [54,56,57]. Consequently, the transcription of HAMP gene is induced by phosphorylated SMADs bind to SMAD4, that in nucleus interact with BMP responsive elements (BMPREs) at HAMP promoter [58,59]. Moreover the membrane proteins HFE and TfR2 could regulate hepcidin expression in response to iron levels (Figure 2). Under iron homeostatic conditions, TfR1 binds HFE on epatocyte cell surface [60]. TfR1 binds also iron loaded transferrin (Fe_2-Tf) with a higher affinity; the overlapping binding site for HFE and Fe_2-Tf,if iron plasma levels increase, causes the dissociation of HFE from TfR1

that consequently could bind TfR2 [51,61] with the final effect of trigger HAMP expression [62].

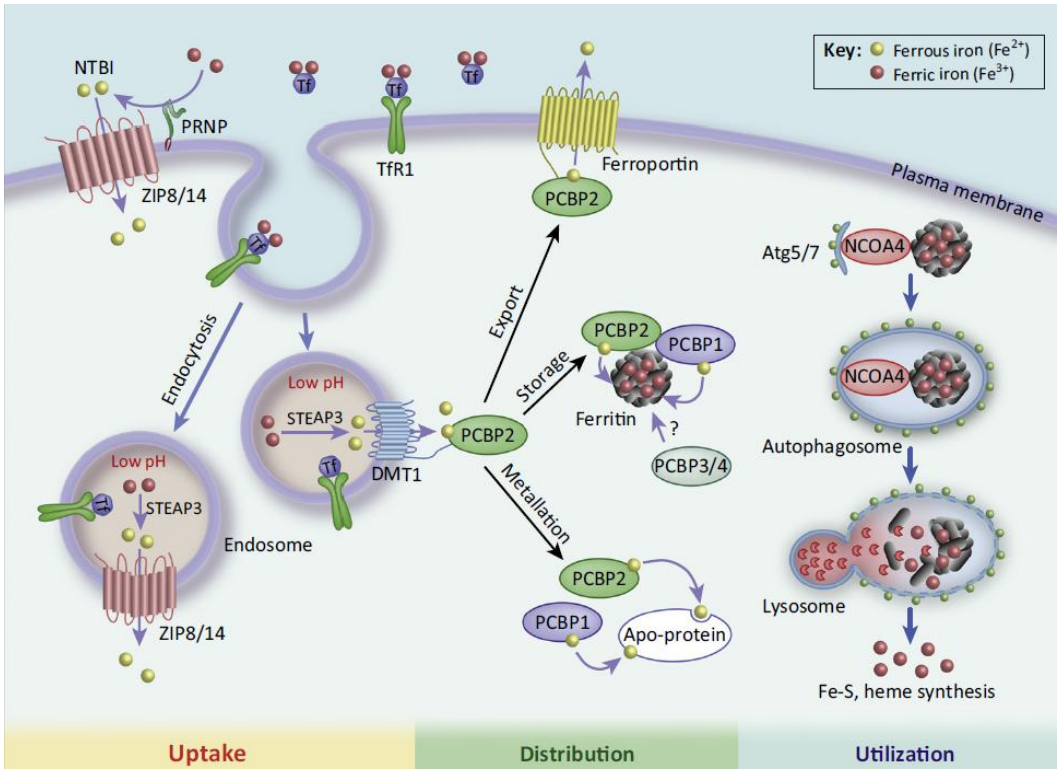

Figure 2. Mechanisms regulating iron metabolism in the cell. ZIP family transporters, ZIP8 and ZIP14, are fundamental for transporting NTBI after reduction of NTBI by prion protein (PRNP). In the acidic endosome, Fe^{3+} is released from Tf and free Fe^{3+} is reduced to Fe^{2+} by STEAP3 and transported to the cytoplasm by divalent DMT1 and ZIP8/14. PCBP1 and PCBP2 are cytosolic iron chaperones that deliver Fe^{2+} to apo-proteins, such HIF (prolyl hydroxylases), ferroportin (iron export), and ferritin (oxidation to Fe^{3+}, storage). NCOA4 mediated autophagy of iron loaded ferritin with the release of iron for utilization in cellular processes. Modified from Bogdan 2016 [53].

Infection and inflammation

All organisms, pathogens included, need iron for survival and proliferation. During infection, pathogens utilize the iron pool of the host. The immune system responds to pathogen with several innate and adaptive mechanisms, among these hypoferremia has a host defence function [49]. During infection, the iron concentration in the plasma may decrease from the physiological range of 10-30 μM to 1-3 μM [63]; also at lower concentration iron is strongly bound to Tf, inaccessible to pathogen iron transporters, limiting the generation of NTBI that can be promptly used by many microorganisms

[63]. Hepcidin promotes all mechanisms responsible for hypoferremia during inflammation and infection [64]. In fact hepcidin levels are greatly increased during infection and inflammation [63]; due to hepcidin increase, Fpn1 endocytosis and degradation promotes low iron absorption from diet and high deposition of iron in macrophage and storing cells [1]. In particular, increased iron scavenging and macrophage storage play a key role in evading iron to pathogens and protecting the host from the toxic effects of increased levels of iron, heme and hemoglobin that could result from tissue damage during infection and inflammation [63]. The presence of pathogens during infection induce macrophage and other cell type to recognize "non self" and to induce the secretion of pro-inflammatory cytokines, as interleukin (IL)-6, -22 and type-1 interferon (IFN) [49,64-66]. All these cytokines trigger the expression of HAMP gene, in particular binding TLR on the membranes of hepatocytes and leukocytes and stimulating Jak-signal transducer and Stat3 pathway [67]. Thus extracellular pathogens are deprived of iron.

Moreover innate immunity engages also other proteins than hepcidin able to relocate and sequester iron useful for host defence [63]. In particular lactoferrin, an homologue of Tf that differs for the capacity to bind iron also at low pH, a typical milieu of inflamed and infected tissues; haptoglobin transports free Hb, hemopexin transports heme to macrophages and hepatocytes for degradation. Nramp1 is an iron transporter of Fe^{2+} found on membranes of phagocytic vacuoles of macrophages and neutrophils [63]. All these proteins, involved with iron binding or transport, show an increased expression during infection and inflammation; their synthesis is cytokines induced (i.e. Nramp1 is induced by LPS and IFNγ) [68].

Hypoxia

Red blood cells and, consequently, the O_2 transporter hemoglobin are produced via erythropoiesis. During hypoxia, low body oxygen levels induce erythropoiesis. Iron metabolism and erythropoiesis during hypoxia are modulated by hypoxia inducing factor (HIF) [69] (Figure 2). HIFs are transcription factors that bind hypoxia-response elements (HREs), controlling the expression of Tf, TfR1, and CP, as well as of HMOX, SLC11A2, CYBRD1 and EPO (the genes responsible for the expression of HO1, DMT1, DcytB and erythropoietin, respectively) resulting in enhanced intestinal

iron uptake, inhibition of HAMP expression in the liver, through a HRE-mediated mechanism [70-73].

Anemia and erythropoiesis

Ineffective erythropoiesis mimics a hypoxic condition observed during anemia. Erythropoietin (Epo) is a glycoprotein hormone mainly synthesized in the adult kidney [74]. Its functions is primarily inhibition of apoptosis of erythroid precursors [69]. Hypoxia is able to increase largely Epo production. Hypoxia regulates Epo and consequently erythropoiesis, the down-regulation of hepcidin expression during anemia is a consequence not only of hypoxia but also of erythropoiesis itself. In fact, a new hormone produced by erythroblasts in response to EPO during erythropoiesis- erythroferrone- plays a role in hepcidin level reduction [1] (Figure 2).

Cellular regulation

Hepcidin is fundamental in the systemic regulation of iron metabolism. Moreover other mechanisms exist at cellular level to regulate genes involved in iron metabolism. Among these the modulation of general cellular mechanisms that promote alternative transcript variants (i.e. alternative transcription initiation, polyadenylation and splicing) and more specific systems able to control the stability of the mRNAs and proteins involved in iron homeostasis [1].

IRON METABOLISM DISORDERS

Notwithstanding a perfect regulation in body iron homeostasis, iron overload or deficiency conditions could be induced by genetic, physiological or environmental factors. In the presence of an iron overload the consequence is the iron deposition in liver, heart and other tissues [75]. If the overload is due to increased dietary absorption the deposition occur in the liver, with a gradient from the periportal hepatocytes to the centrilobular hepatocytes. If iron overload is due to an uncontrolled release from macrophages, iron accumulates at mesenchymal level [76]. Iron overload disorders are genetic or acquired. Hemochromatosis, aceruloplasminemia, and atransferrinemia are genetic disorders with iron overload [76]. Acquired iron loading diseases originate from a secondary iron overload not due to mutation in genes involved directly in iron homeostasis.

Several types of anemia-genetic or acquired- are due to iron deficiency. Iron deficiency anemia (IDA), anemia of chronic diseases (ACD) and the iron-refractory iron-deficiency anemia (IRIDA) are typical iron deficiency pathologies [77-79].

Iron overload disorders

Hereditary hemochromatosis (HH) is the most frequent iron overload disease, show an excessive parenchymal iron deposition in several organs, as liver, heart and pancreas. All hereditary forms lead to the same pathological mechanism of entry of higher amounts of iron to the plasma to support iron-depending processes, i.e. erythropoiesis. Higher amounts of iron in plasma induce primarily increased Tf saturation and iron deposition at several organs, with long term consequences: cirrhosis, hypogonadism, cardiomyopathy, arthropathy, diabetes and hepatocellular carcinomas [80]. In HH hepcidin level is abnormally low although high levels of iron in circulation [81-85]. HH is divided in four types for clinical outcomes and genes affected: HFE-related HH, juvenile hemochromatosis (JH), TfR2-associated hemochromatosis and ferroportin disease. The HFE-related HH is the mildest form (90% of total cases of HH), characterized by a gradual deposition of iron in organs along life [80]. It is characterized by elevated Tf saturation and sFt levels. The majority of the individuals with hemochromatosis are actually homozygotes for p.C282Y. This substitution avoid the formation of the disulfide bond between C225 and C282 residues, essential for HFE association with beta2-microglobulin(β2M) [81]. The hepcidin expression is deregulated because p.C282Y mutated HFE protein is unable to bind to β2M and to be transported to the cell surface where it would interact with TfR1 and TfR2 [1]. JH is a rare disease of iron overload metabolism. It is mainly due to mutations in the HJV and HAMP genes [82,83]. It presents a severe iron overload caused by full saturation of Tf, high sFt levels and iron deposition [80]. The third type of HH is due to mutations in TfR2 gene; characterized by increased TfSat and sFt [80,85]. The last type of HH, also named ferroportin disease, is an iron overload disease with mutations in the SLC40A1 gene. There are two different form of disease: form A- ferroportin mutants are unable to export iron from cells leading to cellular (especially macrophage) iron accumulation with decreased availability of iron for serum Tf (low saturation level) [80]. Form B: ferroportin mutations cause a gain of function with normal iron export capacity but

insensibility to hepcidin downregulation, consequently iron is constitutively absorbed and released by cells, resulting in increased Tf saturation and parenchymal iron overload [84]. Mutations in CP gene generate another rare iron metabolism-related disease named aceruloplasminemia. Main symptoms of aceruloplasminemia are brain iron deposition, retinal degeneration, ataxia and dementia for its essential role in brain iron metabolism [87]. Mutations in Tf gene generate atransferrinemia, a microcytic and hypochromic anemia with tissue iron overload, increased sFt and low levels of Tf [88]. Aceruloplasminemia and atransferrinemia were rare and recessive disorders.

Iron deficiency pathologies

IDA is the most common nutritional deficiency worldwide, frequently occurs in premenopausal woman, children, hospitalized individuals or caused by an iron-poor diet [89]. Individual with permanent state of inflammation for chronic disease present ACD [78]. During inflammation, IL-6, a pro-inflammatory cytokine produced by macrophages, induce the expression of hepcidin and, consequently, low dietary iron absorption and stored iron release [90] causing anemia. There are also congenital anemia disorders; among these, IRIDA, characterized by congenital microcytic and hypochromic anemia, low MCV, Tf saturation, no response to iron administration, recessive transmission [91]; caused by mutations in the MT2 gene (TMPRSS6) [92]. Matriptase-2 physiologically inhibits hepcidin expression causing the cleavage of membrane Hjv; IRIDA patients show extremely high levels of hepcidin, consequently iron absorption by the gut is impaired [93].

CHAPTER 2

Dictyostelium discoideum

THE ORGANISM

Dyctiostelium discoideum (Dd) belongs to the social amoebae (Dictyostelia). Phylogenetically, Dictyostelia form a subgroup in amoebozoa, one of the kingdoms of eukaryotes [94]. *Dd* is evolutionarily distant from yeast and humans, at the edge between unicellular and multicellular organism, as the name "social" suggest; its genome sequencing indicates that is closer to animals and fungi than to plants [95].

Dd lives in deciduous forest soil and moldy leaves where feeds on bacteria, yeast and other microorganisms that are engulfed by phagocytosis [96]. Normally, during vegetative growth stage, *Dd* grows as a single-cell amoebae independent, using simple mitotic divisions for its duplication. If depletion of food occurs (starvation), a developmental program started with several changes in gene expression [97]. Cells aggregate by chemotaxis, caused by secretion of cAMP. The derived aggregate is multicellular, with peculiar differentiation and morphogenetic characteristics (Figure 3). The microenvironment starvation finally leads to the formation of a fruiting body consisting of spore and stalk cells. Stalk cells are dead vacuolated cells, whereas spore cells are resistant to extreme temperatures or food scarcity. If favorable environmental conditions occur, new amoebae will be born from the spores [94] (Figure 3).

DYCTIOSTELIUM DISCOIDEUM AS ANIMAL MODEL

Human macrophages and neutrophils are immune cells that recognize, engulf pathogens and after destroy them in intracellular vesicles. These leukocytes employed chemotaxis to reach pathogens and phagocytosis for eliminate them [98]. These behaviors are utilized also by *Dictyostelium discoideum*, to track and ingest bacteria as its food source. Consequently, studies of *Dd* provide insights into chemotaxis and phagocytosis of immune cells with the simplicity of this eukaryotic organism [99].

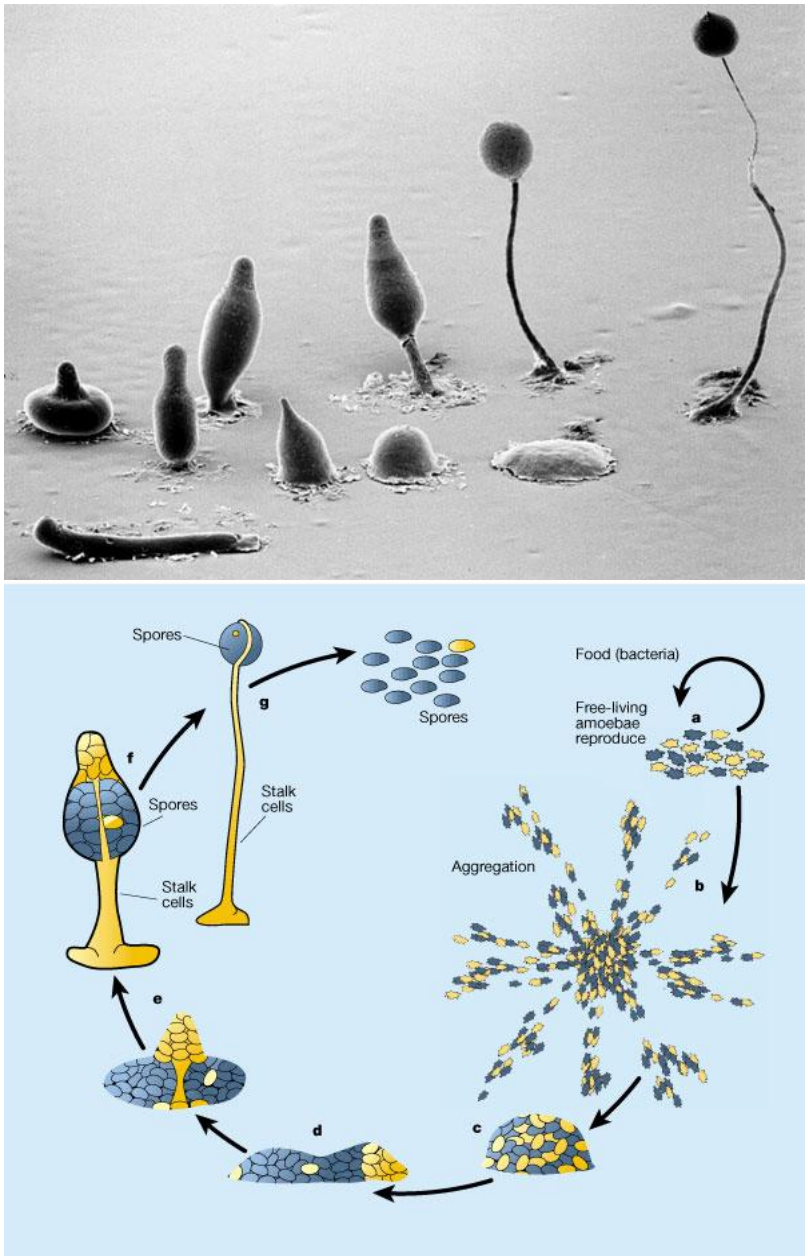

Figure 3. Stages of the *Dictyostelium discoideum* life cycle. Upper panel: a typical microscopy image of the *Dd* life cycle; Lower panel: the schematic summary of the life cycle: Free living amoebae (A); aggregate due to cells chemotaxis toward cAMP released from neighbor cells (B); formation of aggregates with increasing complexity (C, D, E); culmination stage (F); fruiting body (G). (images from http://www.ailab.si/supp/bi-visprog/dicty/dictyExample.html).

The phagocytosis process starts with the binding of pathogen to receptors on the leukocyte membrane; this interaction causes a reorganization of actin cytoskeletal components in the cell, resulting in the internalization of the pathogen and the formation of a phagosome [100]. This vescicle matures by the fusion with endocytic and lysosomal vesicles, shaping the phagolysosome, where the ingested pathogen is destroyed. Basic aspects of chemotaxis and phagocytosis are evolutionarily conserved between human and simple eukaryotic organisms like *Dd* [101-103].

In mammals, phagocytosis by macrophages and neutrophils remove pathogens or apoptotic cells. In *Dd*, the same process is essential for acquiring nutrients from the surrounding environment. Many intracellular pathogens elude phagolysosomal fusion with the intent to avoid lysosomal destruction [104]. Mammalian macrophages, neutrophils, and *Dd*, show similar molecular components involved in phagocytosis and phagosome maturation. These findings suggest that pathogens able to escape killing in mammalian phagocytes are also capable to avoid phagocytosis mediated by *Dd*, suggesting common targets in both cell types [99] and the ancient evolution of the phagolysosomal apparatus [100,105,106]. Thus, Dictyostelium's strategies to neutralize pathogens are expected to be of general relevance [107]. Consequently, *Dd* has become a model organism for studying how host resists to infection or the pathogen escape defense strategies [108].

DYCTIOSTELIUM DISCOIDEUM: PROFESSIONAL PHAGOCYTE AND PATHOGEN HOST

All eukaryotes, independently from the complexity of the organism studied, show similar mechanism in the host pathogen interaction [99,109,110]. Pathogens must interfere with the maturation process of the phagosome to survive and to obtain a replication niche in the host, in the same phagosome or escaping in the cytoplasm [111]. Normally bacteria are ingested by *Dd* with phagocytosis or macropinocytosis with the formation of large vesicles on the plasma membrane. After engulfment in the cell, the phagosome or macropinosome fuses with acidic vesicles containing V-H^+ ATPase and other vesicles with Nramp1 protein exposed on the membranes [112-115]. Many pathogens, i.e. Legionella and Mycobacteria, interfere with the endocytic pathway avoiding fusion of the pathogen-containing phagosome with acidic and

lysosomal vesicles, enhancing the association with different compartments of the cell, such as endoplasmic reticulum [116], mitochondria [117], generating a replication vacuole. Legionella, due to massive intracellular growth, produce cell lysis, whereas Mycobacteria escape intact cells with non-lytic exocytic mechanism [118]. Intracellular survival of pathogens depend also from ion acquisition; i.e. *S. typhimurium* virulence relies on Mg^{2+}, Mn^{2+}, K^{+} and Zn^{2+} [119-122]; others bacteria as Salmonella, Legionella and Mycobacteria accumulate large amounts of iron, as Fe^{2+} is an essential metal for all cells [123-125]. Iron deprivation induces the expression of siderophores for iron recovery in pathogens. In order to defeat bacteria, a divalent metal transporter-Nramp1-depletes the phagosome of iron exploiting a proton gradient [115, 126]. Disruption of Nramp gene augment sensitivity to infection in *Dd*, increasing intracellular growth of Legionella or Mycobacteria. In fact, also mutations in this transporter are associated to innate susceptibility to mycobacterial diseases and *S. typhimurium* infection [127-129]. Study in *Dd* on gene expression of Nramp1 showed increased intracellular growth of *L. pneumophila* and *M. avium* if gene inactivation occurs, while *L. pneumophila* growth is completely inhibited by its overexpression [115]. *L. pneumophila* inhibits the recruitment of the $V\text{-}H^{+}$ ATPase in vacuoles containing bacteria, without a direct effect on Nramp1 recruitment. Indirectly, the absence of the vacuolar ATPase inhibit the proton gradient necessary for iron depletion due to Nramp1 [116].

IRON TRANSPORTERS IN BACTERIAL INFECTION

Iron homeostasis is fundamental for the resistance to pathogen bacteria in higher eukaryotes as in *Dd.* Iron is necessary for *Dd*, its deficiency or overload reduce *Dd* cell growth. In mammals like in *Dd* many genes regulate iron homeostasis. SLC11A family includes the two iron transporters, namely natural resistance associated membrane protein 1 (Nramp1) and 2 (Nramp2).

The Nramp family is distributed in evolutionarily different organisms, from bacteria to humans [126]. In mammals, Nramp1 (SLC11A1) expression is limited to the lysosomal membrane of mature macrophages, granulocytes and monocytes [130] *Dd*Nramp1, like mammalian ortholog, is expressed only in phagosomes and

macropinosomes. The protein derived from transGolgi and is rapidly associated to phago- or macropinosomes, and is then recycled from the vesicles after lysosomal maturation [115]. Nramp1 is a symporter for H^+ and divalent metal ions out the lysosome; this action removes iron and other metals fundamental for intracellular pathogens to activate their virulence genes [131]. Moreover another metal transporter-Nramp2 (SLC11A2, or DMT1)-is present on plasma membrane of several tissues; mutations in the mammal Nramp2 transporter are associated to severe microcytic anemia, serum and hepatic iron overload [126,132]. In *Dd*, Nramp2 is localized as membrane protein in the contractile vacuole, which regulates osmolarity. The presence in different compartments of Nramp1 and Nramp2 suggests that both transporters jointly play a role in iron homeostasis.

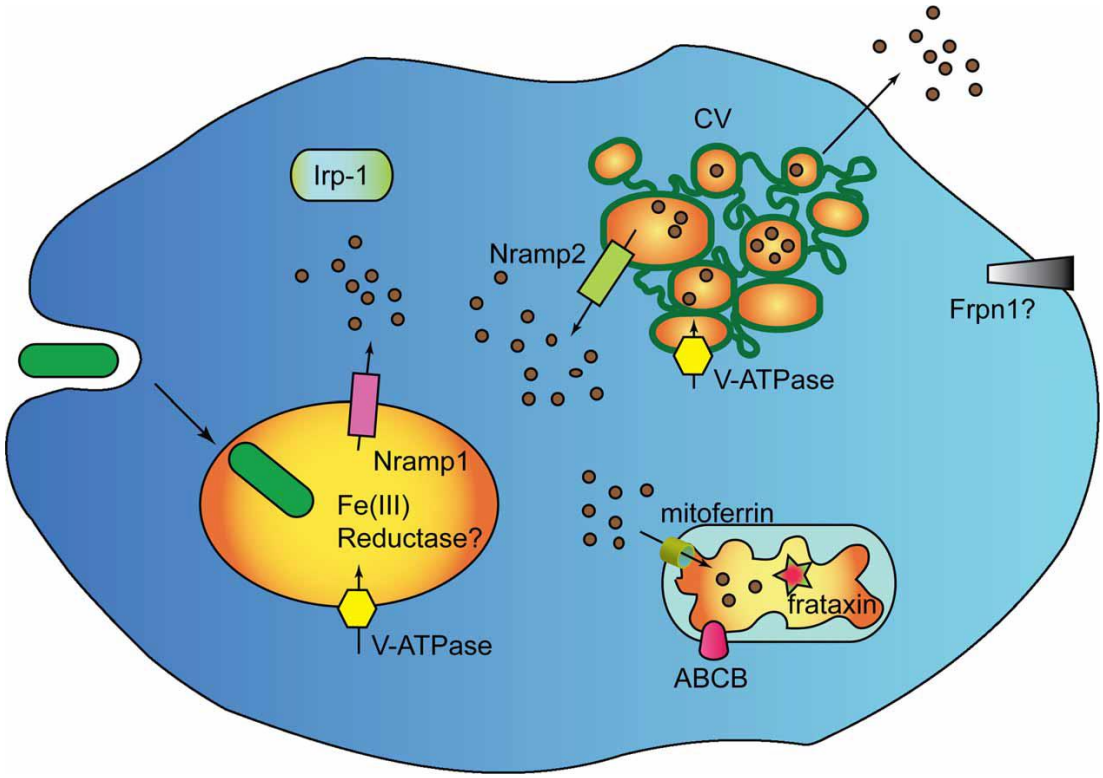

Figure 4. Model for Nramp1 activity in *Dyctiostelium discoideum*. Nramp1 and the V-H^+ ATPase colocalized in phagosomes rapidly after their uptake. The activity of the vacuolar ATPase generates a proton gradient in the maturing phagosome that provides the electrogenic force necessary for Nramp1 to transport iron or other divalent metals, to the cytoplasm, thus depleting bacteria from an essential nutrient element. From Bozzaro 2013[108].

Eukaryotic SLC11A proteins transport Fe^{2+}, $Mn^{2+}$and Co^{2+} [131,133], whereas for bacterial homologs (MntH subfamily) Mn^{2+} is the main substrate [134,135]. In *Dd* iron is not absorbed with membrane transporters, but it is obtained by destruction of phagocyted bacteria and release via Nramp1 from phagosomes to the cytoplasm (Figure 4).

In *Dd* the $V\text{-}H^{+}$ ATPase pumps protons inside the lumen of the contractile vacuole [136,137]; moreover the same $V\text{-}H^{+}$ ATPase is localized also in phagosomes and macropinosomes after phagocytosis [137,115] suggesting that the vacuolar ATPase provide the electrogenic potential necessary for transport activity of both Nramp1 and Nramp2 [126,131,133]. In *Dd*, depletion from phagosome of iron via Nramp1 could be an efficient mechanism of the host to starve the pathogen for iron. On the contrary, pathogen (i.e. Legionella) could prevent co-localization of the vacuolar ATPase avoiding acidification of the vacuole, inhibiting Nramp1-dependent iron efflux, even favoring iron influx for pathogen benefit [116]. In prokaryotes, three different manganese transporters (MntH) are related phylogenetically to the Nramp proteins [138], the crystal structure for one of them has been recently determined [139]. Homologs of Nramp in yeast, Smf1 and Smf2, transport iron and also manganese, whereas a third one, Smf3, probably transports iron from the vacuole to the cytosol [140,141].

CHAPTER 3
SOLUTE CARRIER PROTEINS (SLCs)

Membrane transporters expression is diffused all over the body, greatly in epithelia of liver, intestine, kidney, and other organs with barrier functions (brain, testes and placenta) [142]. Their presence ensure cellular homeostasis of fundamental substrates. Pumps, ATP binding cassette (ABC) superfamily and the solute carrier (SLC) superfamily are the main transporter category; pumps and ABC transporters use ATP hydrolysis for their (in many cases) uphill transport. SLC transporters are crucial for the uptake of small molecules into cells. SLC transporters are mostly facilitative or secondary-active; specifically depend on electrochemical gradient to facilitate substrates movement across membranes, or on gradients of ion created by ATP-dependent pumps to transport substrates against its concentration gradient [142].

MEMBRANE TRANSPORTERS

Transporters are fundamental for the uptake in cells and organelles of sugars, amino acids, nucleotides, inorganic ions and drugs [143]. Their mechanism of function sort them in: passive transporters (or facilitated transporters) that permit solute diffusion down their electrochemical gradient; active transporters that produce solute gradient employing mechanism that supply energy (Figure 5).

The active transporters are subdivided in: “primary active” transporters, ATP-dependent, such as ABC transporter family and ion pumps (ATPases).

Mammalian ABC transporters utilize ATP for the transport of different substances (ions, carbohydrates, lipids, xenobiotics and drugs) out of cells or into cellular organelles [144].

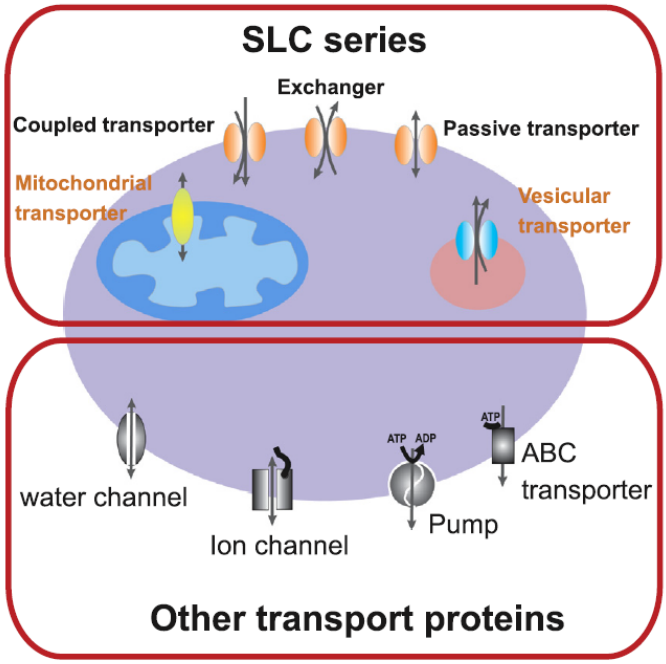

Figure 5. SLC and non-SLC transporters. All transporters are expressed in the plasma membrane or in intracellular compartments. Modified Hediger 2013 [143].

Ion pumps use ATP to actively pump Na^+, K^+, H^+, Ca^{2+} and Cu^{2+} out of cells or into organelles (145-147]. These pumps also maintain electrochemical ion gradients across membranes that are used by ‘‘secondary-active’’ ion-coupled transporters to drive uphill nutrients transport across cellular membranes. Channels, similar to transporters, permit solute movement down their electrochemical gradient [148-151]. Transporters show a fixed stoichiometry of ions/solutes per cycle of transport; channels, on the contrary, depend on its open probability due to gate control and its conductance (amount of charges per second at a given voltage).

SOLUTE CARRIER (SLC) MEMBRANE TRANSPORT PROTEINS

SLC membrane transport proteins are essential for their physiological functions, such as nutrient uptake, ion transport, and waste removal [152]. Membrane transporters play a key role in the regulation of small-molecule transport across membranes regulating cell’s internal physiology and interaction with the environment [153]. The SLC superfamily is the largest group of protein transporters, which includes 456 members in the human genome, divided in 52 subfamilies phylogenetically grouped [143]. SLCs are localized on the cell surface and in organellar membranes as integral proteins; their molecular mass is 40-90 KDa, the aminoacidic sequence range is 300-800 residues

[154]. SLCs are principally facilitative transporters and secondary active transporters (symporters and antiporters). In the superfamily there is a wide variety of transporters.

SLC nomenclature and classification

The systematical study of all the genes encoding SLC clarifies their evolution from common ancestral genes and permit their classification in subfamily on the basis of sequence identity. In the 1990s Matthias Hediger created the SLC gene nomenclature system to simplify the characterization of different types of mammalian transport of the SLC series [155]. Genes are called using the acronym SLC, followed by a number (i.e. SLC11, solute carrier family 11), followed by a letter for subfamily definition (A is used if the family is not subdivided) and a last number defining the single transporter gene (e.g., SLC11A1). Transporters are included in a specific family when the corresponding protein show at least 20% amino acid sequence identity to other members of the same family [143]. About 10% (~2000) of all human genes are transport-related, highlighting the biological significance of transporters in cell homeostasis. The SLC families are a significant portion of these genes since that 400 genes coding for SLCs.

Structural biology of SLCs

All membrane proteins together correspond to one third of the whole proteome and two thirds of all current therapeutic targets; unfortunately the number of structures deposited in Protein Data Base is exceptionally small, representing less than 1% of all available 3D structures. Hydrophobic segments of integral membrane proteins show complicated expression and crystallization. Those crystal structures derived mainly from atomic structures of SLC homologs from eukaryotes (i.e. the Drosophila dopamine transporter DAT (SLC6A4) [156] and prokaryotes (e.g., the *Shewanella oneidensis* di-/tri-peptide transporter PEPTso (an SLC15 homolog)[157]. These structures share sequence identity of ~30% or more and conserved binding site with human homologs, useful models for studying substrate specificity of the human SLCs. The SLC members show different structure, consisting of a variety of folds, many not related to each other [158]. Leucine transporter (LeuT) and the Major Facilitator

Superfamily (MFS) are the most diffuse structure in the human SLCs (Figure 6A and 6C).

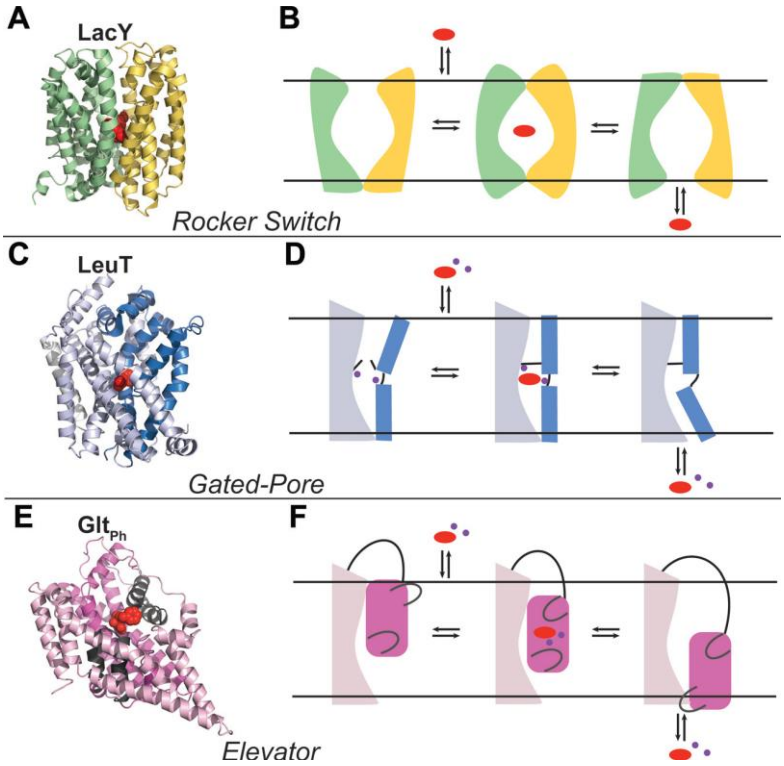

Figure 6. Transport mechanism models. In each case, a transporter structure that uses the mechanism described is shown in (A,C,E) and transport cycle of the associated transporter are shown in (B, D, F): outward-open, occluded and inward-open. **Rocker switch. (A)** LacY is shown in an outward-open bound conformation with the N- and C-terminal halves in green and yellow, respectively, and the substrate in red. **(B)** The substrate binds to a V-shape conformation on the extracellular side of the membrane, inducing an intermediate occluded state. The substrate is then released from an inverted V-shape inward-open conformation. **Gated-pore. (C)** LeuT in outward-open bound conformation, with the scaffold and bundle domains in light and dark blue, respectively, the substrate and ions in red and purple. **(D)** The scaffold domain remains static, whereas the bundle domain undergoes conformational changes to bind and release the substrate. The binding site is enclosed by a thin gate (i.e. a salt bridge) on the extracellular side, and a thick gate (TM1) on the intracellular side. **Elevator. (E)** Glt_{Ph} in outward-open bound conformation, with the oligomerization and transport domain represented in light pink and magenta, respectively, and the two gates (HP1 and HP2) in gray. The inhibitor is shown in red, and sodium ions in purple. **(F)** The oligomerization domain remains invariant while the transport domain moves in a piston-like movement to transport the substrate from the extracellular side to the intracellular side of the membrane. Modified Colas 2016[158].

The MFS model contains 12 transmembrane helices (TM) arranged into two inverted structural pseudo-repeats of six TMs. The MFS structure is one of the most diffuse in nature, i.e. the glucose facilitative transporters GLUTs/SLC2 and the proton

oligopeptide cotransporter family SLC15 display this structure. LeuT structure have 10 TMs, with 2 five-TM inverted pseudo-repeats, where the first two TMs in each of the two repeats (i.e., the 'bundle domain') are twisted relative to the three remaining TMs of the repeat (i.e., 'scaffold domain'). The SLC5 family of Na^+/glucose transporters and the SLC6 family of Na^+/Cl^- dependent neurotransmitter transporters show LeuT structure [158]. Knowledge of the structures of membrane proteins could be useful to better understand their functional mechanisms.

Functional mechanisms of SLCs

The SLC transporters utilize different energy coupling mechanisms to mediate movement across the membrane; they comprise secondary active transporters, ion channels (the ammonium channel SLC42), and other membrane proteins such as SLC51B and members from the SLC3 family able to transport only with other SLC members (SLC51A and SLC7 members, respectively) creating functional heterodimers. Transport by SLC transporters is a dynamic process mainly due to an "alternating access" model. In this mechanism, the transporter alternates between outward and inward conformations, with several intermediate states (i.e. an occluded state, with the binding site not accessible) [158]. Three major types of alternating access mechanisms have been described for SLC transporters (Figure 6): -rocker-switch. The N- and C-terminal halves of the transporter move back and forth from an outward facing state to an inward facing state, perpendicular to the membrane. Transporters with an MFS structure transport substrates via the rocker-switch mechanism, i.e. the *E. coli* Lactose Permease LacY (Figure 6A and 6B) [159,160]; -Gated-pore. The binding site is enclosed by two gates [161]. Opening of the outward-facing gate enables the substrate binding, the substrate release happens in the cell by the opening of the second gate in the cytosol. Proteins with LeuT structure utilize this mechanism [162-164] (Figure 6C and 6D); -Elevator. The domain containing the binding site, namely transport domain, moves along the axis perpendicular to the membrane, whereas an oligomerization domain remains inert (Figure 6E and 6F). Glt_{Ph} displays elevator mechanism, is a trimer with different conformations [165-167].

Transporters, diseases and pharmaceutical perspective

There is increasing interest in SLCs because of their genetic link to human diseases; 190 different SLCs have been found mutated in human disease [168]; more than 400 SLC genes are associated with human diseases. Moreover, due to the important role of transporters in normal physiology and disease, several transporters are fundamental for pharmaceutical perspective. In fact transporters could be used as drug targets or as a mechanism to help drug delivery to cells and tissues [152].

THE SOLUTE CARRIER 11 (SLC11) FAMILY

Members of the SLC11 (Nramp) family transport iron and other transition-metal ions across cellular membranes. The natural resistance-associated macrophage protein (Nramp) homologs constitute the SLC11 family, proton-coupled transporters that facilitate the cellular absorption of divalent metal ions (such as Mn^{2+}, Fe^{2+}, Cd^{2+}, Co^{2+}, Zn^{2+}, Ni^{2+}, and Pb^{2+}) [169]. These membrane proteins are present in all kingdoms of life with a high degree of sequence conservation [170]. The mammalian SLC11 family is comprised of two members, SLC11A1 and SLC11A2. These proteins share 66% identity and 82% similarity in amino acid sequence, and are part of the large SLC11 family of integral membrane proteins expressed in evolutionarily different organisms [169]. In general, SLC11 proteins are transporters that employ the proton electrochemical gradient as driving force to transport divalent metal ions, in particular transition metal ions [11,133,171].

SLC11A1: Natural resistance-associated macrophage protein 1 (Nramp1)

SLC11A1 is a 90-100 kDa integral transmembrane protein expressed in the lysosomal compartment of macrophages and in tertiary granules of neutrophils. The encoded integral membrane protein is composed of 12 predicted transmembrane domains (TMD, Figure 7). SLC11A1 is coexpressed with the lysosomal-associated membrane protein 1 (LAMP1), a marker of the late endosomes/lysosomes of resting macrophages [172]. During the maturation process of the phagosome, both proteins are recruited to the phagosomal membrane in particular when stimulated by inflammatory signals [173]. The human SLC11A1 gene was localized to the long arm of chromosome2

(2q35); polymorphisms in the NRAMP1 gene are associated with various immune diseases [126]. NRAMP1 plays a key role in innate resistance against infection mediated by intracellular bacteria, its main function is the regulation of intraphagosomal metal concentration, in particular of iron and manganese to limit microbial survival and replication [169]. Human SLC11A1 shows an expression profile analogous to mouse ortholog and was consequently associated to resistance to infections of different intracellular pathogens. A single loss of function mutation (G19D) in the predicted TM4 of mouse Nramp1 is associated with an augmented susceptibility to infections with Mycobacterium, Salmonella, and Leishmania [174].

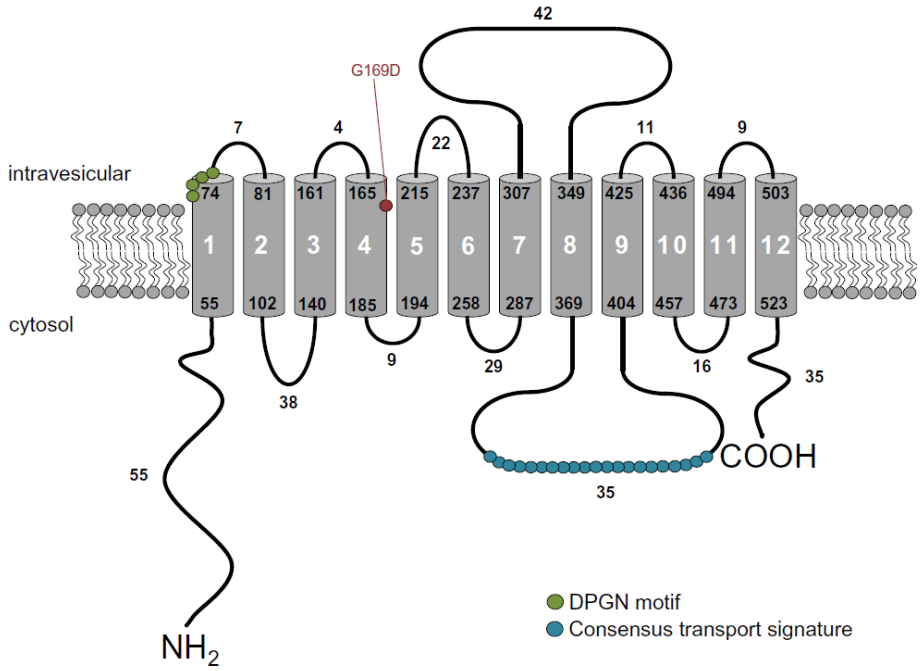

Figure 7. Secondary structure representation of SLC11A1. Consensus transport signature (blue) and DPGN motif (green) are shown in the representation of SLC11A1. The mutation (G169D, in red) in mice leads to infection susceptibility. White numbers in grey cylinders indicate the transmembrane regions; black numbers indicate the first and last amino acid of each TMD. Modified Montalbetti 2013 [169].

The role of Nramp1 in innate immunity is a function evolutionarily ancient, since that Nramp gene upregulation after infectious stimuli is already present in fish,

invertebrates, and plants, and moreover functional data on the amoeba *Dictyostelium discoideum*, an animal model to study professional phagocyte [115].

SLC11A2: Divalent metal transporter-1

The other element of the SLC11 family is Nramp2 (SLC11A2, DMT1, DCT1); this transporter is ubiquitously expressed, mainly in duodenum, immature erythroid cells, brain, placenta and kidney [169]. Nramp2 play a key role in iron absorption at the apical membrane of enterocytes [11] following SLC40A1 mediates basolateral iron exit in circulation. Moreover Nramp2 is involved also in the iron recycling from the hemoglobin destruction after macrophage phagocytosis of senescent erythrocytes [169]. Last role of Nramp2 is the iron transport in the cytoplasm, due to its expression on endocytotic vesicles during TfR-mediated cellular iron uptake [175]. Nramp2 exists in different isoforms, depending on alternative splicing of the 3'-terminal exon; the two isoforms show different C-terminal amino acid and an iron response element (IRE) in the isoform I -absent in the isoform II- in 3' UTR mRNA [176]. Nramp2 isoform I is mainly on apical membrane of epithelial cells (duodenum, kidney) [68,177], whereas isoform II, with a different C-terminus (25 amino acid residues), is predominantly involved in iron recycling endosomes [175]. The importance of Nramp2 for iron metabolism appears evident since that mutations impairing Nramp2 function cause congenital microcytic hypochromic anemia and serum and hepatic overload in human [126]. Moreover, in two animal models of iron deficiency, mk mouse [178] and Belgrade rat [18], Nramp2 mutations (G185R in TM4) cause a severe iron deficiency and microcytic anemia with impaired intestinal iron absorption [18,178]. The SLC11A2 gene encodes a protein of 560–570 amino acid, the native SLC11A2 protein of 65 kDa, but the transporter expressed in the cell results 90–100 kDa due to a N-glycosylation, necessary for plasma membrane expression; the predicted SLC11A2 topology (Figure 8) shows 12 putative TMDs and intracellular N- and C-terminal [169].

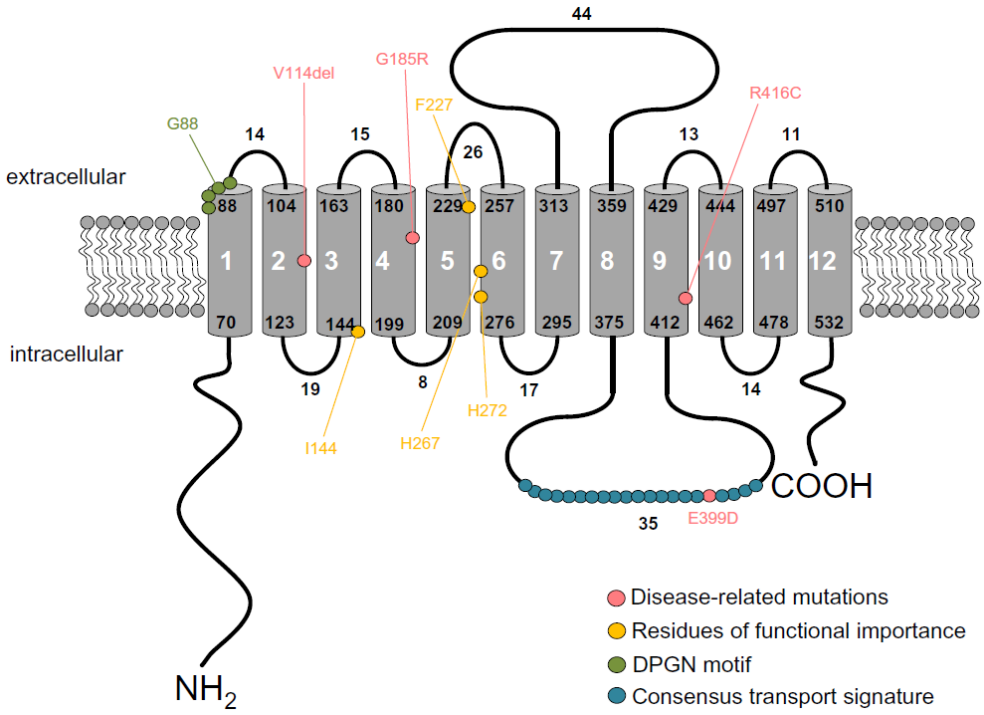

Figure 8. Schematic secondary structure representation of SLC11A2. Highlighted circles shows the locations of known human mutations resulting in microcytic anemia (pink), the DPGN motif (green), consensus transport signature (blue), and residues directly involved in the transport mechanism of SLC11A2 (yellow). The amino and carboxyl-termini are denoted by NH2 and COOH, respectively. White numbers in grey cylinders indicate the proposed transmembrane regions; black numbers indicate the first and last amino acid of each TMD. Modified Montalbetti 2013 [169].

Crystal structure of SLC11 transporters

The determination of the crystal structure of *Staphylococcus capitis* DMT (ScaDMT) in 2014 gives new information about the determinants of ion selectivity; this prokaryotic homolog of the SLC11 transporters shows, similar to LeuT, an inward-facing conformation with a substrate-binding site in the center of the transporter [139]. In particular, the first five α-helices are structurally related to the following five α-helices by a two-fold rotation around an axis in the center of the membrane [162] (Figure 9B and 9C). As in LeuT, the first helix of each repeat (i.e., α-helices 1 and 6 in ScaDMT) is unwound in the center of the membrane, creating a niche where residues interact with transported substrates. Conserved mechanism for transition-metal ion selectivity in all SLC11 family and homologs is suggested since mutations of

interacting residues affect ion binding and transport in both ScaDMT (37% are identical, 59% are homologous to human protein) and human DMT1. Due to functional characterization and high sequence homology, bacterial SLC11 homologs share structure and substrate specificity with eukaryotic counterparts suggesting similar transport mechanisms [139]. The biggest differences are found in their termini, which are both longer in DMT1; the 59 additional amino acids on the C terminus encode an additional transmembrane helix, for a total of 12 TMD for DMT1 and 11 TDM for ScaDMT (structure and topology in Figure 9).

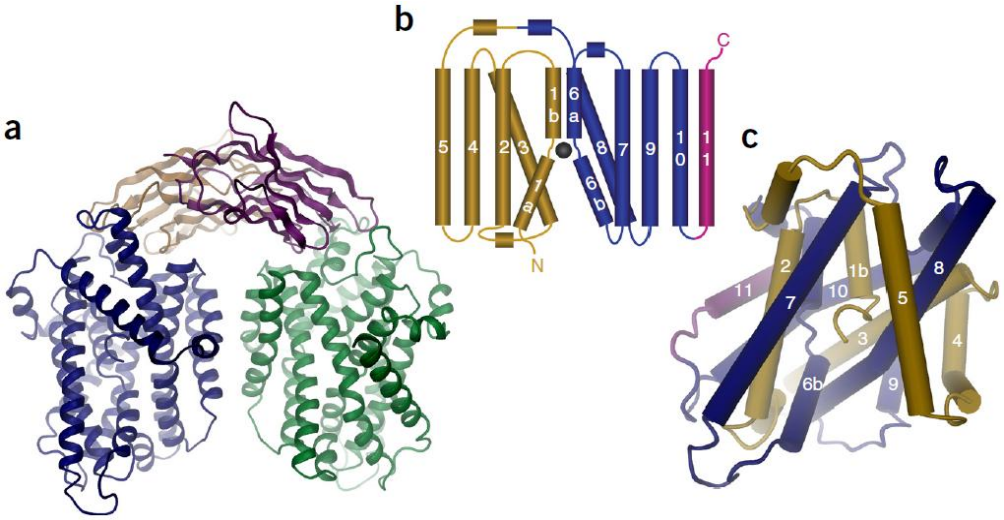

Figure 9. ScaDMT structure. (a) Ribbon representation of ScaDMT. (b) Topology and (c) structure of ScaDMT. The two halves of the protein are in brown and blue, and helix 11 is in magenta. Helices are represented as cylinders. In the topology, the bound ion is a grey sphere in the metal ion-binding site. The ion is surrounded predominantly by harder ligands along with the soft sulfur of Met226. This binding model is valid for all the family members since interacting residues are strongly conserved. Modified Ehrnstorfer 2014 [139].

The binding site is constituted of conserved residues, able to coordinate divalent transition metals (Mn^{2+}, Fe^{2+}, Cd^{2+} and others) but not alkaline earth metal (Ca^{2+}, Mg^{2+}) [132,179]. This is essential because high concentration of alkaline earth metal in the duodenum would interfere with the fundamental absorption of Fe^{2+} [171]. This specific selectivity for transition metals is due to the presence of an unusual but conserved methionine. The evolutionary pressure to maintain the methionine is explained because it increases the selectivity for transition metal transport even with the prevalence of calcium and magnesium [171].

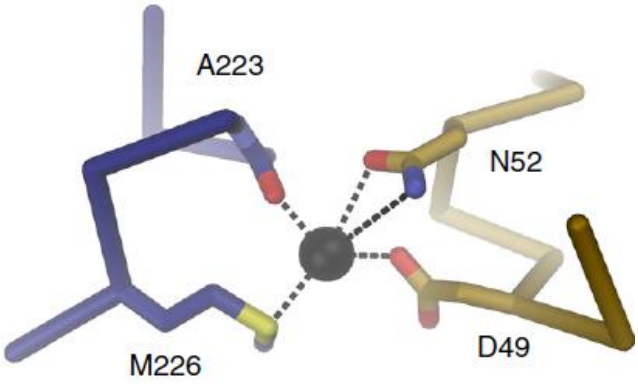

Figure 10. Ion coordination. Transition metal ion coordination in the binding site. Interactions are indicated by dashed lines. Modified Ehrnstorfer 2014 [139].

Moreover other residues in the binding site are important for divalent transition metals interaction (Figure 10), i.e. Mn^{2+} is coordinated by the carbonyl oxygen of the peptide bond linking residues 223 and 224 at the C-terminal end of α-helix 6a; the side chain of Met226 of the same helix; and side chains of Asp49 and Asn52 from the near α-helix 1 (Figure 10); the conserved His233 is implicated in pH regulation and proton transport [180,181]. Fe^{2+}, Co^{2+}, Ni^{2+}, Cd^{2+} and Pb^{2+} occupy the same binding site of Mn^{2+}; the binding of Cd^{2+} and Pb^{2+} suggests the uptake mechanism for these toxic heavy metals [139]. In Figure 11 is described the transport mechanism of ScaDMT.

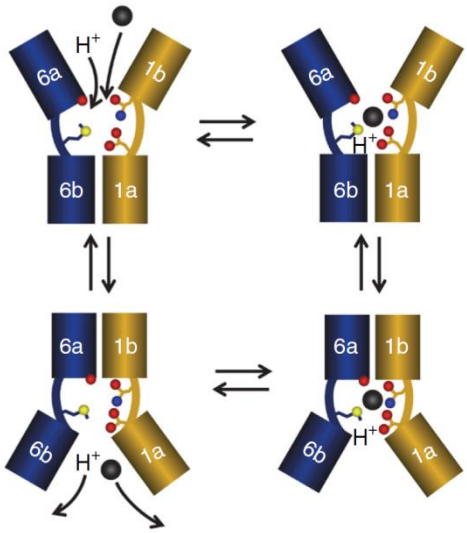

Figure 11. Transport mechanism. Binding of a proton and a transition metal ion to a site accessible from the outside is followed by a conformational change of the two halves of α-helices 1 and 6 around a hinge located at the ion binding region. The rearrangement closes the extracellular pathway and opens an intracellular pathway to the ion binding site. Caused by this conformational change, the two substrates are released into the cytoplasm, and the empty transporter returns to its outward facing state. Ehrnstorfer 2014 [139].

Structure-function studies of Nramp metal ion transporters

Electrophysiological studies of SLC11A2 expressed in Xenopus oocytes revealed that SLC11A2 is rheogenic and transports a wide range of divalent transition metal ions (Cd^{2+}, Co^{2+}, Cu^{2+}, Mn^{2+}, Zn^{2+}). At physiological membrane potentials (-90 to -30 mV) human and rat SLC11A2 display high affinity for Fe^{2+} ($K_{0.5}$ circa 2 μM at pH 5.5) and H^+ ($K_{0.5}$ circa 1 μM) [181]. Kinetic analysis showed that SLC11A2 transports Fe^{2+} with H^+ in a coupled state with a stoichiometry of 1:1. However, uncoupled Fe^{2+} or H^+ currents (leak) through SLC11A2 were observed depending on extracellular pH (pH_e). At neutral pH_e, 50 μM Fe^{2+} evoked inward currents not accompanied by a H^+ influx [180] suggesting that Fe^{2+} transport is predominantly uncoupled from H^+ under these extracellular conditions. Steady-state and presteady state currents were observed following step-changes in membrane potential at pH_e 5.5 in the absence of substrates. Moreover, acidifying pH_e from 7.5 to 5.5 in the absence of Fe^{2+} results in an inward current and intracellular acidification in SLC11A2 expressing oocytes [11]. Presteady-state currents were pH dependent and inhibited in the presence of substrates, such as Fe^{2+} [180]. Interaction between Nramp2 and protons generate changes in protein conformation and presteady-state currents.

Site-directed mutagenesis studies of SLC11 homologs highlighted important residues for cation transport, situated in different TMDs. Amino acids with particular properties (i.e. charges, histidine, and glycine), once mutated, inhibit the transport [126]. The TMD1 C-terminal end and adjacent external loop1/2 are important for metal binding, uptake, and for proton coupling [126]. Also histidyl residues in TMD6 (Nramp2 His267, and His272) are essential for metal/proton uptake and proton-dependent interactions; mutations at these sites maintain substrate uptake, but separate it from proton transport [126]. Also, TMD2 and 4 are implicated in SLC11A2 metal ion transport, permeability, and selectivity. A single F227I mutation in TMD4 abolished the proton slip through SLC11A2 without effect on metal ion transport [182], whereas the I144F mutation in TMD2 inhibited substrate transport and increased slip currents [183].

*dd*Nramp1 and *dd*Nramp2 showed aminoacidic sequence quite different, while most species harboring two or more homologs of Nramp [184]. *dd*Nramp1 belongs, with all

metazoan Nramp proteins, to the archetypical Nramp subfamily, whereas Nramp2 is closer to prototypical Nramp proteins like aquatic protists, fungi and proteobacteria (i.e. MntH Cα subclass) [138,174,184]. Functional studies on *dd*Nramp1 could contribute with novel insights on the mechanism of action of the mammalian ortholog, whereas similar studies on *dd*Nramp2 could suggest a role of the homologous proteins in protists, and help to clarify the possible function of the contractile vacuole in divalent metal homeostasis. *dd*Nramp1 and *dd*Nramp2 had different aminoacidic sequences and were localized in different intracellular location, but both proteins colocalize with the V-H^+ ATPase, suggesting that divalent metal transport is strongly associated to proton transport, as demonstrated in other members of SLC11 family. For *dd*Nramp1, iron uptake studies performed with purified phagosomes demonstrated a vacuolar-ATPase-dependent transport [115]. Cell lysis and difficulties to obtain isolated and functional vacuole vesicles did not permit similar experiments with *dd*Nramp2. Aim of this study would be, however, to know if *dd*Nramp2 is involved in iron influx or efflux across the vacuole, and to characterize the different metal transport specificity and regulation of the two iron transporters of *Dyctiostelium discoideum*, *dd*Nramp1 and *dd*Nramp2.

MATERIALS AND METHODS

IN SILICO ANALYSES

All DNA sequences, obtained from NCBI database (www.ncbi.nlm.nih.gov), were analyzed with the following bioinformatic tools:

Homology information	BLAST http://blast.ncbi.nlm.nih.gov/Blast.cgi
Alignments	CLUSTAL O http://www.ebi.ac.uk/Tools/msa/clustalo/
Restriction enzymes analyses	WEBCUTTER 2.0 http://rna.lundberg.gu.se/cutter2/
ORF identification	ORF finder http://www.bioinformatics.org/sms2/orf_find.html
Analysis of different codon usage	Rare Codon Calculator % Min-Max http://www.codons.org/

SYNTHESIS OF CHIMERIC cDNA

In order to generate chimeric cDNA: the main coding sequence of the two transporters homologs of SLC11 family, namely Nramp1 and Nramp2 of *Dyctiostelium discoideum* (*dd*Nramp1 and *dd*Nramp2) was attached to portion of N-(59 amino acids) and C-terminus (19 amino acids) of rat DMT1 (*r*DMT1) to facilitate the expression of *dd* proteins on the oocyte membrane. Briefly, to create chimeric cDNA the restriction sites HpaI at the N-terminus (position +96 and +291 for *dd*Nramp1 and *dd*Nramp2, respectively) and NsiI at the C-terminus (position +1533 and +1749 for *dd*Nramp1 and *dd*Nramp2, respectively) were inserted by PCR amplification in cDNA coding for the transporters in pGEMT plasmid (see Table1 for primer sequences). On the other hand, *r*DMT1 (NP037305.2) in pSPORT-1 was mutagenized by site-directed mutagenesis

(Quickchange site-directed mutagenesis Kit, Stratagene Inc., Milan, Italy) with overlapping primers to insert the Eco47III site (at position +171) and the NsiI site (at position +1713). All restriction enzymes were supplied by Promega (Milan, Italy). The chimeric constructs were fully sequenced before cRNA transcription. The resulting chimeric protein is illustrated in Figure 12.

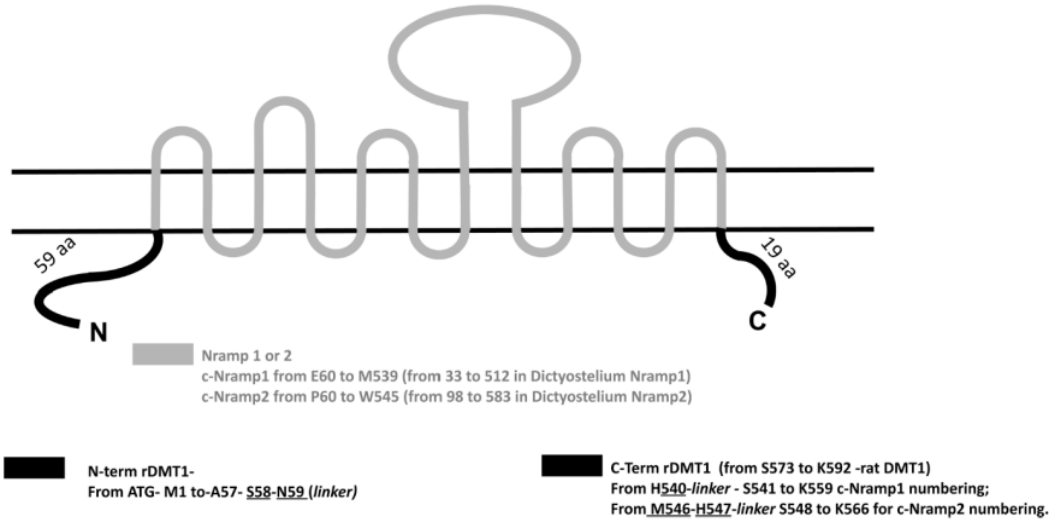

Figure 12. Chimeric protein structure. In grey 12 TMD of *dd*Nramp1 or 2, in black the C- and N-terminus of *r*DMT1. For each protein is described the relative position of amino acids and "linker" amino acids.

The resulting chimeric Nramp1 (c-Nramp1) in pSPORT-1 vector generate a protein with the first 59 amino acids of *r*DMT1 replacing the 32 residues at the N-terminus of *dd*Nramp1 and the 21 C-terminal amino acids replaced by the last 19 amino acid of *r*DMT1. Regarding *c*-Nramp2, the same N- and C-terminus of *r*DMT1 replace the first 97 and the last 46 amino acids of *dd*Nramp2. The particular AT rich sequence of the two *dd*Nramp genes require the following conditions for PCR protocol: DNA 50 ng, 1.25 ng of each primer, dNTPs 0.5mM, 3U of Pfu Taq polymerase , Pfu buffer 10x in 50 µl final volume. Thermocycling conditions: 1' initial denaturation; denaturation (95°C) 1', annealing (60°C) 1', extension (72°C) 3' for 25 cycles, followed by 5' of final extension (72°C).

PRIMER SEQUENCES USED FOR CHIMERIC SYNTHESIS		
pSPORT-1_DMT1_Nsi	**fw**	5'-gttgggcctgtcgttcctggactgtatgcattcggtaagcatct-3'
pSPORT-1_DMT1_Eco47III	**fw**	5'-tcggccagcctcggtgccagcgctcctgcttacagcaac-3'
HpaI_*dd*Nramp1	**fw**	5'-gcccGTTAACgaaaaccctttaataatagaaagtgg-3'
NsiI_*dd*Nramp1	**rev**	5'-CACTGCAGAACCAATGCATagaattaaagttttcttgacccattG-3'
HpaI_*dd*Nramp2	**fw**	5'-gcccGTTAACccatttcaagatagagatagtaatattgg-3
NsiI_*dd*Nramp2	**rev**	5'-CACTGCAGAACCAATGCATccataataataaacaacataaagcaattG-3'

Table 1. Primer sequences utilized forsynthesis of chimeric proteins. In capital letter different enzyme restriction sites.

MUTANTS OF CHIMERIC Nramp2

Mutations in c-Nramp2 were obtained by site-directed mutagenesis following manufacturer's instruction. Briefly, 20 ng of the plasmid pSPORT-1 containing the c-Nramp2 wild type cDNA were amplified with 3U of Pfu Taq polymerase in the presence of overlapping primers to insert the mutated codons (Table 2).

PRIMER SEQUENCES USED FOR c-Nramp2 MUTANTS SYNTHESIS		
Mutant c-Nramp2 A133E	**fw**	5'-tggatccaggtaattgggaaacagatttagaaggtgg-3'
	rev	5'-ccaccttctaaatctgtttcccaattacctggatcca-3'
Mutant c-Nramp2 E137Q	**fw**	5'-ccaggtaattgggcaacagatttacaaggtgggtcaag-3'
	rev	5'-cttgacccaccttgtaaatctgttgcccaattacctgg-3'
Mutant c-Nramp2 A119G	**fw**	5'-aaaattaaaatcatttttaggacctggattatttatatcggtgggatatatgg-3'
	rev	5'-ccatatatcccaccgatataaataatccaggtcctaaaaatgattttaatttt-3'
Mutant c-Nramp2 G125A	**fw**	5'-ctgcattatttatatcggtggcatatatggatccaggtaattg-3'
	rev	5'-caattacctggatccatatatgccaccgatataaataatgcag-3'
Mutant c-Nramp2 S140A	**fw**	5'-gcaacagatttagaaggtggggcaagatttgggtatcaattaa-3'
	rev	5'-ttaattgatacccaaatcttgccccaccttctaaatctgttgc-3'
Mutant c-Nramp2 R141M	**fw**	5'-caacagatttagaaggtgggtcaatgtttgggtatcaattaatgtgggta-3'
	rev	5'-tacccacattaattgatacccaaacattgacccaccttctaaatctgttg-3'
Mutant c-Nramp2 T293V	**fw**	5'-ggttaaatagtgatagtgttatggttgcagttggcatcgttggtgc-3'
	rev	5'-gcaccaacgatgccaactgcaaccataacactatcactatttaacc-3'
Mutant c-Nramp2 T299V/T300V	**fw**	5'-ggttgcaactggcatcgttggtgctgtcgttatgccccataatttgtttttacat-3'
	rev	5'atgtaaaaacaaattatggggcataacgacagcaccaacgatgccagttgcaacc-3'
Mutant c-Nramp2 F306Y	**fw**	5'-cactatgccccataatttgtatttacatggtagtgtggtg-3'
	rev	5'-caccacactaccatgtaaatacaaattatggggcatagtg-3'
Mutant c-Nramp2 A133E/E137Q	**fw**	5'-ggatccaggtaattgggaaacagatttacaaggtgggtcaagattt-3'
	rev	5'-aaatcttgacccaccttgtaaatctgtttcccaattacctggatcc-3'

Table 2. Different primer sequences used for generating c-Nramp2 mutants.

cRNA TRANSCRIPTION

For cRNA transcription, the cDNA encoding the desired protein cloned into the pSPORT-1 plasmid was linearized with NotI, and cRNA synthesized *in vitro* in the presence of Cap Analog 10mM and T7 RNA polymerase 200U. All enzymes were supplied by Promega (Milan, Italy).

OOCYTE PREPARATION AND cRNA INJECTION

Oocytes were obtained from adult females of *Xenopus laevis* (Envigo, Bresso, Italy). The frogs were anaesthetized in MS222 1g/L (tricaine methansulfonate) solution in tap water and portions of the ovary were removed through an incision on the abdomen. The oocytes were treated with 0.5 mg/ml collagenase Type IA (Sigma, Milan, Italy) in ND96 calcium-free solution for at least 30' at 18°C to remove follicular cells and debris. Collagenase activity were stopped with repeated wash steps in ND96 calcium-free solution and NDE. After 24h at 18°C in NDE, the healthy looking oocytes were injected with cRNA diluted in sterile water (0.5µg/µl), using a manual microinjection system (Drummond Scientific Company, Broomall, PA). The oocytes were then incubated at 18°C for 3-4 days in NDE before electrophysiological or different transport studies. The experiments were carried out according to institutional and national ethical guidelines (permit nr. 05/12).

XENOPUS LAEVIS OOCYTE SOLUTIONS

The oocyte (ND96 and NDE) solutions used during oocyte preparation and cultures had the following composition (in mM), ND96: NaCl 96, KCl 2, $MgCl_2$ 1, $CaCl_2$ 1.8, HEPES 5, pH 7.6; NDE: NaCl 96, KCl 2, $MgCl_2$ 1, $CaCl_2$ 1.8, HEPES 5, pyruvate 2.5, gentamicin 250 µg/ml. The external control solution for electrophysiological studies contained in mM: NaCl or TMACl, 98; $MgCl_2$, 1; $CaCl_2$, 1.8, HEPES or MES 5. The final pH values of 5.5 or 7.6 were adjusted with NaOH or TMAOH respectively. The external control solution used for XLOs technique is identical but with addition of Ascorbic acid 1mM.

ELECTROPHYSIOLOGY AND DATA ANALYSIS

Electrophysiological studies were performed using the two-electrode voltage-clamp technique (TEVC, Oocyte Clamp OC-725B, Warner Instruments, Hamden, CT). Intracellular glass microelectrodes were filled with 3M KCl and had tip resistances between 0.5–4MΩ. Agar bridges (3% agar in 3M KCl) connected the bath electrodes to the experimental chamber. The holding potential (V_h) was -40mV. Recording was conducted at a fixed voltage. Transport currents were determined by subtracting the records in the absence of divalent metal ion (external control solution) from the corresponding ones in its presence. Clampex 10.2 (Molecular Devices, Sunnyvale, CA) was used to perform the experiments. Data were analyzed using Clampfit 10.2 (Molecular Devices). Figures and statistics analysis were prepared with Origin Pro 8.0 (Microcal Software Inc., Northampton, MA).

IMMUNOCYTOCHEMISTRY

Immunocytochemistry techniques were utilized on oocytes previously tested on TEVC, in order to verify the correct expression of the transporters on the plasma membrane. Oocytes were washed twice with ND96 and fixed with 4% paraformaldehyde in ND96 (15' at 4°C); then washed at RT with ND96 in mild agitation (5' at RT, 3 times). Finally fixed oocytes were included in Polyfreeze tissue freezing medium (Polysciences, Eppelheim, Germany) and immediately frozen in liquid nitrogen. Cryosections were obtained with a Leica CM 1850 cryostat (thickness 7 µm) and preserved at -20°C until tested. Sections were rehydrated with PBS 10' at RT, incubated in blocking buffer (2% bovine serum albumin, BSA (w/v), 0.1% Tween in PBS) at RT for 30', and then over-night at 4°C with the primary antibody, rabbit anti-c-Nramp1 or c-Nramp2 from *Dictyostelium discoideum* (polyclonal antisera purified, kindly donated by Bozzaro and coworkers), diluted 1:200 in blocking buffer. Samples were washed with blocking buffer 5' for 3 times at RT. Cryosections were then incubated with the secondary antibody, 0.5mg/ml diluted 1:250 in blocking buffer (CyTM 3-conjugated Goat Anti-Rabbit, Abcam, Cambridge, UK), at RT for 45' and again washed with blocking buffer 5' for 3 times at RT. Images were observed with a

fluorescence microscope Olympus BH2 through a rhodamine filter set (excitation/emission filters 550/580nm). Images were acquired with a DS-5M-L1 Nikon digital camera system.

XENOPUS LAEVIS OOCYTE SMOOTHIE (XLO_S)

XLO_S is a powerful technique to study divalent metal transporters (i.e c-Nramp1, c-Nramp2 or *r*DMT1 as positive control) expressed in *X. laevis* oocytes with the fluorophore calcein, able to quench in presence of different divalent metal ions (Figure 13). To verify the divalent metal transport across *Xenopus laevis* membranes expressing c-Nramp1, c-Nramp2 or *r*DMT1, control oocytes or injected with the specific cRNA, were injected with 50 nl of calcein 12.5 µM (Sigma-Aldrich, St Louis, MO) dissolved in intracellular solution (KCl 130mM, NaCl 4mM, $MgCl_2$ 1.6mM, EGTA 5mM, HEPES 10mM, glucose 5mM, at pH 7.6) 4 days after cRNA injection. Following fluorophore entry, the oocytes were incubated for 1h in external control solution at pH 5.5 or pH 7.6 in the presence or absence of $MnCl_2$, $FeCl_2$ and $CoCl_2$ 100µM. After 3x wash in ND96, oocytes were crushed in presence of ND96+SDS10% and centrifugated 5' at maximal speed. Clear supernatants were plated and measured on a microplate reader Infinite 200 (Tecan Group Ltd., Männedorf, Switzerland) at λ 485 nm for excitation, and λ 535 nm for emission (given the spectrum of the fluorophore calcein). The results were obtained in arbitrary units of fluorescence (AU).

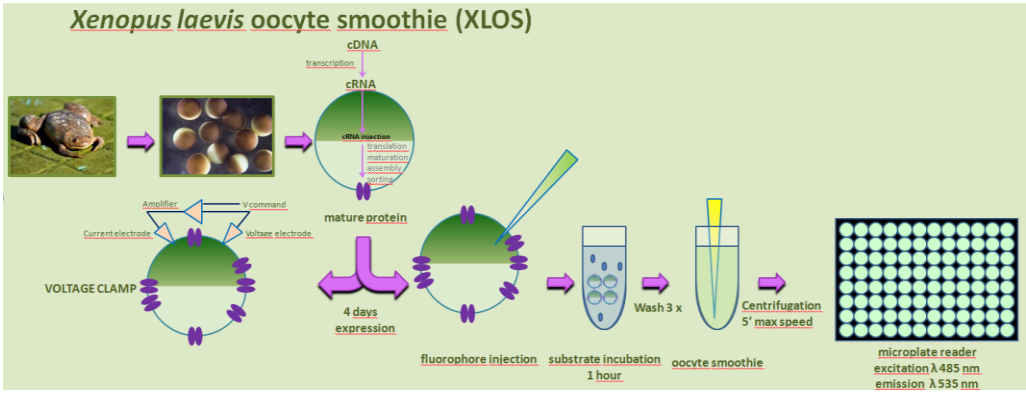

Figure 13. Schematic representation of XLO_S technique. An alternative technique to evaluate the entry of divalent metal ions across membrane transporters, particularly useful to study non-electrogenic transporters.

RESULTS

CHIMERIC PROTEINS SYNTHESIS

First, to characterize the function of iron transporters of *D. discoideum*, *dd*Nramp1 and *dd*Nramp2 has been expressed in *X. laevis* oocytes using an appropriate expression vector. The original proteins *dd*Nramp1 and *dd*Nramp2 resulted in a very low level of functional expression when tested with TEVC, not surprisingly since that in *D. discoideum* are not plasma membrane proteins. To increase their expression on plasma membrane of oocytes, the N and C-termini of both proteins were replaced with the N- and C-termini of rat DMT1. This transporter kindly provided by Marciani and coworkers is well expressed in *X. laevis* oocytes as previously published [11,180,185,186], moreover, in our research work it was utilized as positive functional control. Electrophysiological characterization require good levels of expression. The chimeric protein between *r*DMT1and *dd*Nramp1 and *dd*Nramp2 has been constructed with 59 amino acids at N terminus and 19 residues at C terminus from *r*DMT1 as well as its 3' untranslated region (UTR) to improve the stability and the expression of *D. discoideum* metal transporters in *X. laevis* oocytes, with the approach previously described for Smf1p [187].

c-Nramp1 AND c-Nramp2 CODON USAGE ANALYSIS

To analyze the real feasibility of the heterologous gene expression of *Dyctiostelium discoideum* genes in our model, we applied the software "*Rare Codon Calculator Min-Max"* to match the different codon usage utilized by *D. discoideum* and *X. laevis*. The analysis assign a value "-100%" if the sequence codify only with rare codons, whereas "100%" means that the sequence is constituted by common codons; "0%" value is attributed if the codon usage is identical to the codon usage of the organism chosen as reference. The Figure 14 of c-Nramp1 (left panel) and c-Nramp2 (right panel) showed the results of the sequence analysis compared with *X. laevis* codon usage. The c-Nramp1 expression in oocytes reaches the min % of -38% in the utilization of rare codons indicating that the protein can be translated but with some difficulty; on the other hand, c-Nramp2 expression displays a min % of "-43%" suggesting higher intrinsic difficulties in the synthesis of this protein.

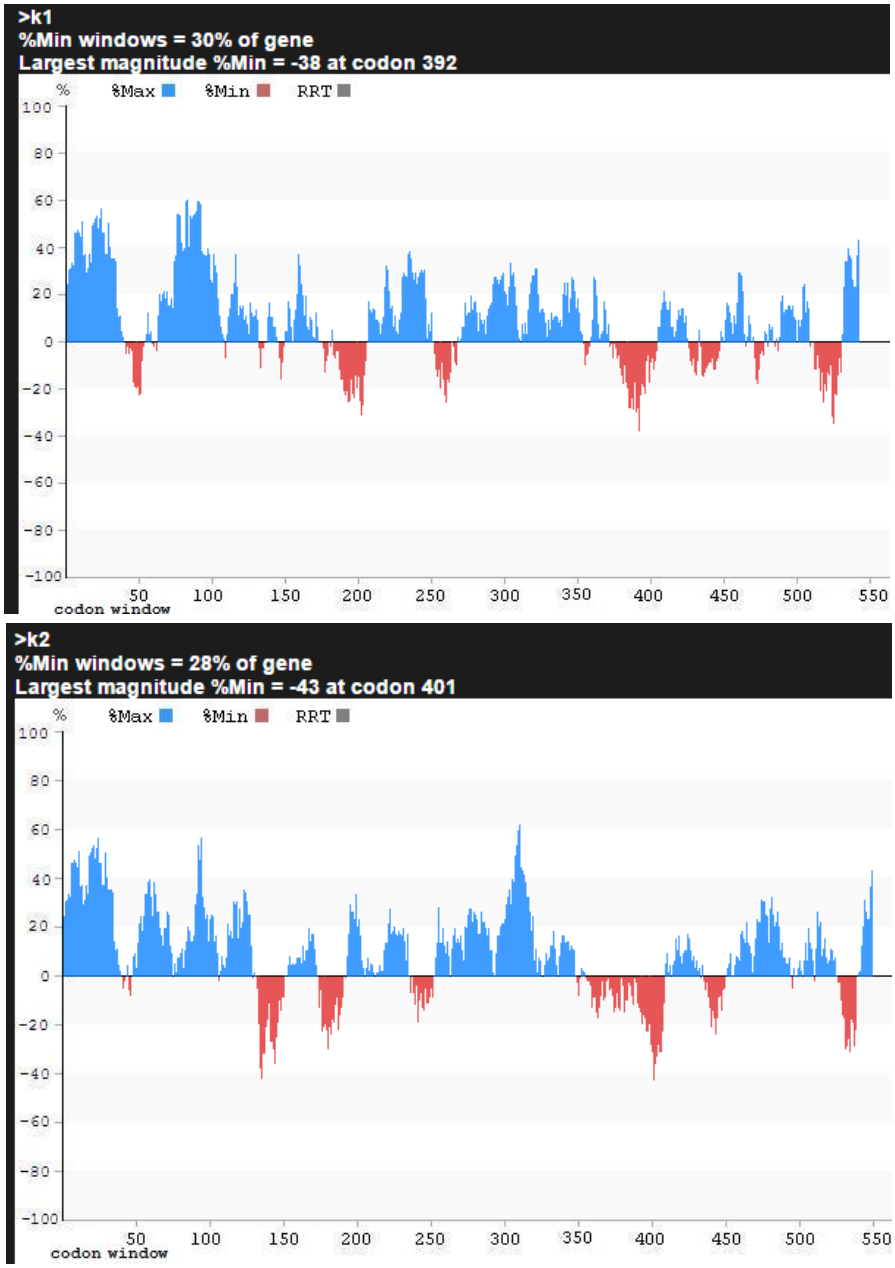

Figure 14 "Rare Codon Calculator Min-Max" analysis for c-Nramp1 (upper panel) and c-Nramp2 (lower panel) compared to *X. laevis* codon usage. Red represents the percentage of rare codons utilized whereas blue identifies common codons.

Dyctiostelium discoideum c-Nramp1 METAL TRANSPORTER: ELECTROPHYSIOLOGICAL CHARACTERIZATION

To characterize the c-Nramp1 metal transporter, the oocytes were tested electrophysiologically by TEVC to verify the presence of transport currents associated with metal uptake.

First, oocytes expressing c-Nramp1 were clamped at a fixed voltage (V_h -40 mV) in external control Na solution (Figure 15) at pH 5.5 and perfused with different concentration (10, 30, and 100μM) of $MnCl_2$ and $FeCl_2$ to determine the optimal concentration to perform the electrophysiological experiments. $FeCl_2$ and $MnCl_2$ were able to elicit inward transport currents also at low concentrations suggesting the high affinity of the transporter for these ions (Figure 15). Since that the currents in any conditions tested were small, the affinity was not determined with a dose response experiment.

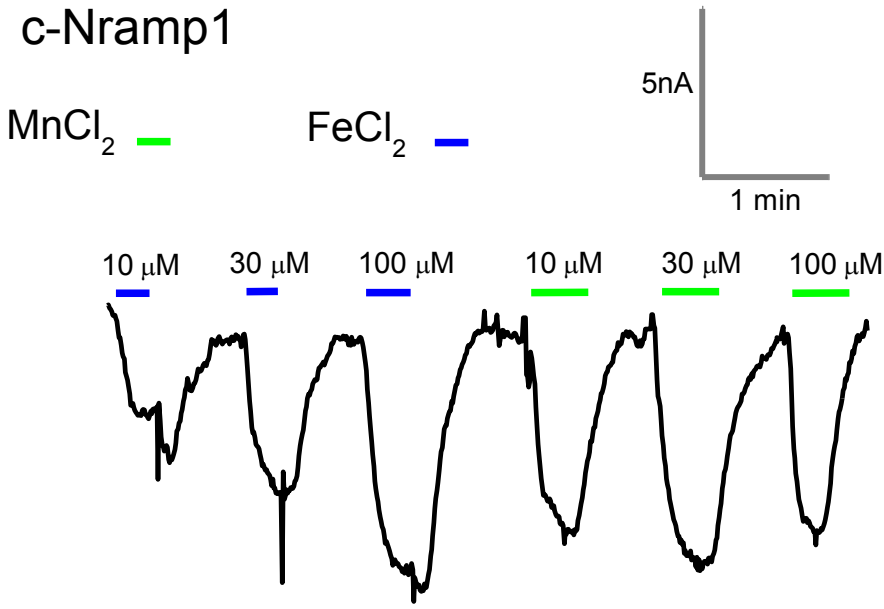

Figure 15. Transport current in c-Nramp1. Metal ion transport currents of $FeCl_2$ and $MnCl_2$ at pH 5.5 in external control sodium solution. Concentration of 10, 30, and 100μM for these two ions were tested. Experiments conducted at fixed voltage (V_h -40mV).

Afterwards, oocytes expressing c-Nramp1 were clamped at a fixed voltage (V_h -40 mV) and tested in Na (Figure 16A) or in tetramethylammonium chloride (TMA) (Figure 16B) solution at pH 5.5 and perfused with different divalent metal substrates (Fe^{2+}, Mn^{2+}, Co^{2+}, Cd^{2+}, Ni^{2+}, Pb^{2+}, Zn^{2+}, all 100µM) to determine ion selectivity. TMA was an impermeant cation, and it was used to test the sodium dependence. Both TMA and Na gave rise to transport current, suggesting that the transporter is sodium independent.

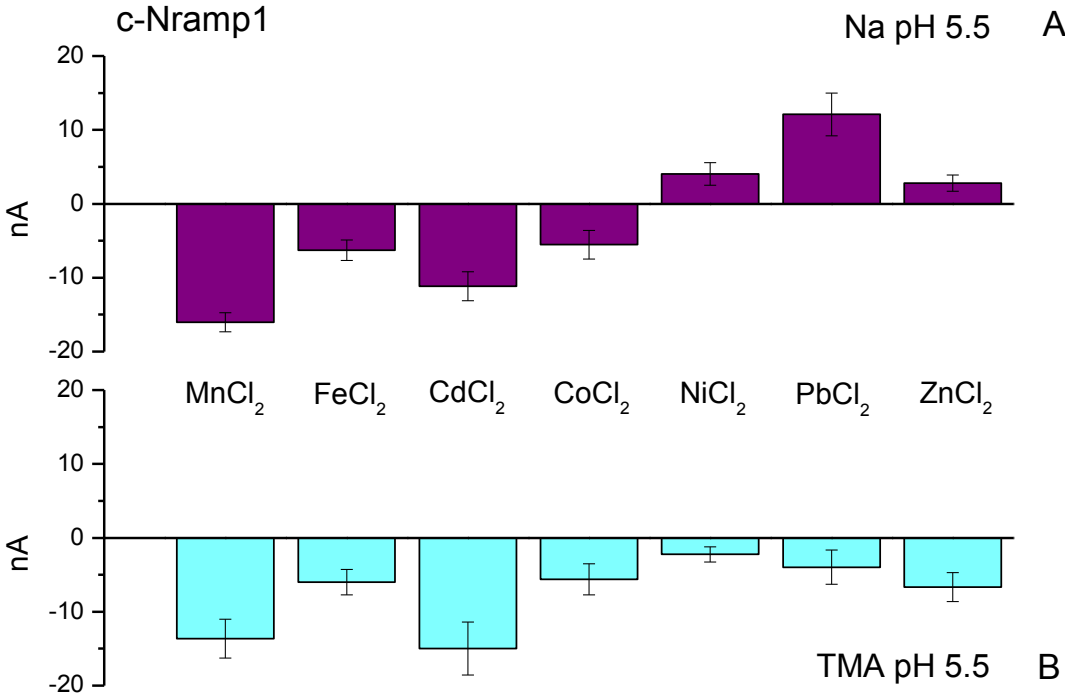

Figure 16. Transport current in c-Nramp1. Metal ion transport currents of 100µM for all divalent ions tested at pH 5.5. Experiments conducted at fixed voltage (V_h -40mV). **A.** External control sodium solution. Mean±SE of 7-50 oocytes, 2-7 batches. **B.** External control impermeant TMA solution. Mean±SE of 3-25 oocytes, 2-5 batches. Transport currents were determined by subtracting the records in the absence of the substrate from the corresponding ones in its presence.

The mean of the transport currents in the presence of different divalent cation showed that Mn^{2+}, Fe^{2+}, Cd^{2+} and Co^{2+} are the substrates that induce the largest transport currents in Na and TMA, whereas Ni^{2+}, Pb^{2+} and Zn^{2+} elicited small inward currents in

TMA solution, and only in sodium solution the same metal ions gave rise to apparent outward currents. This discrepancy could be ascribed to the block of the sodium leak current (Figure 16B) as explained in the following paragraph.

The similar currents elicited by $FeCl_2$ or $MnCl_2$ (Figure 15) suggest to use the latter, that is not oxidizable, to test the pH dependence of the transporter. As shown in Figure 17, in c-Nramp1 and *r*DMT1 expressing oocytes the currents became smaller when pH vary from acidic (5.5) to neutral (7.6) pH and, at pH 7.6 for c-Nramp1 the current became even outward.

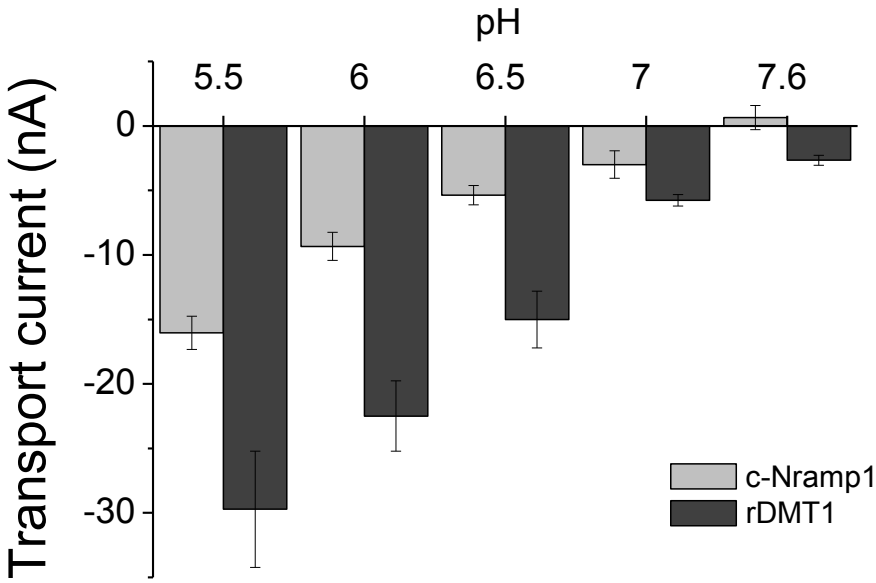

Figure 17. Effects of increasing pH on transport currents of $MnCl_2$ 100µM. Mean±SE of 8-20 oocytes, 3 batches. P<0.05 for c-Nramp1 and *r*DMT1 vs control; P<0.05 for pH 5.5 vs pH 7.6. Mn^{2+} evoked currents mediated by c-Nramp1 and *r*DMT1, which are maximal at pH 5.5, smaller at higher pH and switch outwardly at pH 7.6 for c-Nramp1.

The absence of outward currents at pH 7.6 in TMA demonstrated that this particular behavior may be due to the presence of sodium leak current blocked when the amount of protons, that are coupled to metal transport, is reduced and the Na ions available.

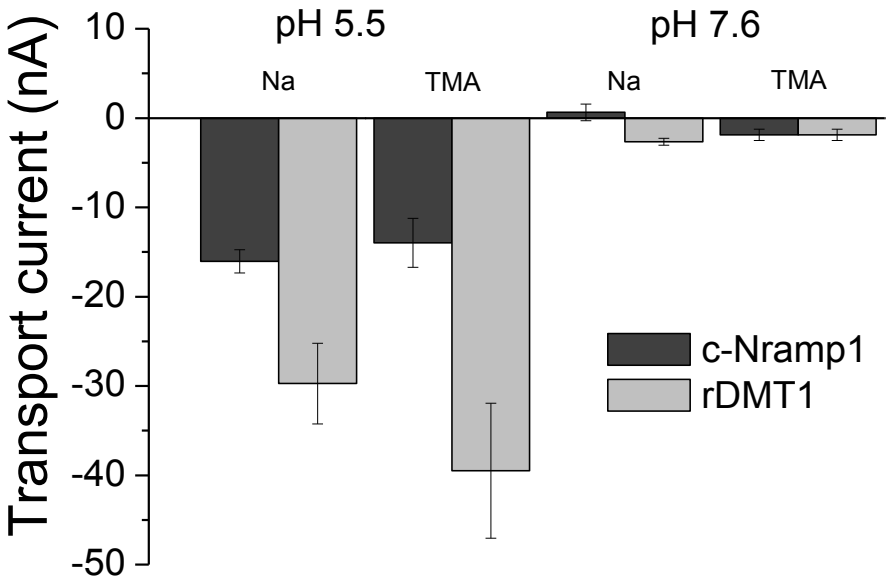

Figure 18. Effects of pH 5.5 or 7.6 on transport currents of $MnCl_2$ 100μM in external sodium or TMA control solution. The outward current at pH 7.6 showed for c-Nramp1 disappears if Na is replaced by TMA, suggesting the presence of a Na leak current that is blocked by the presence of the divalent metal ion substrate. Mean±SE of 10-50 oocytes , 5-10 batches. P<0.05 for c-Nramp1 and *r*DMT1compared to control oocytes or at pH 7.6. Transport currents were determined by subtracting the records in the absence of the substrate from the corresponding ones in its presence.

This particular behavior of c-Nramp1 in sodium solution was previously observed in the yeast Smf1p transporter [187,188]. This kind of current, well described by Nelson [189], is due to the block of the high Na^+ permeation trough the transporter when the proton concentration was lower than that required for the best functionality of the transporter (i.e. pH 7.6). At pH 7.6 the transport of divalent metal ions is anyway coupled to proton, in the absence of substrate (Mn 100μM in this case) Na^+ pass through the transporter in an uncoupled way give raise to a huge current. In the presence of the substrate, the tranporter starts to work in a coupled way, transporting metal ions and proton generating a transport associated current and reducing the Na^+ permeation and consequently its leak current. In figures 15, 17, 18 the amount of transport current was determined by the subtraction of the current in the presence of the substrate from that in its absence, but the last at pH 7.6 is mainly due to Na^+ permeation (leak) and consequently the transport associated current seems outward due

to its small entity compared to the massive Na^+ current. Moreover this particular Na^+ leak current at pH 5.5 reduced its amplitude due to its competition for the same binding site or the same translocation pathway with protons that, in this case, are highly concentrated. Subsequently to characterize the permeation property of the transporter, we recorded the currents in the presence of external solution, where Na was substituted with different cation: Li, K, Rb and Cs at the same concentration (98mM) and in the absence of divalent metal substrates at both (5.5 and 7.6) pH (Figure 19 and 20).

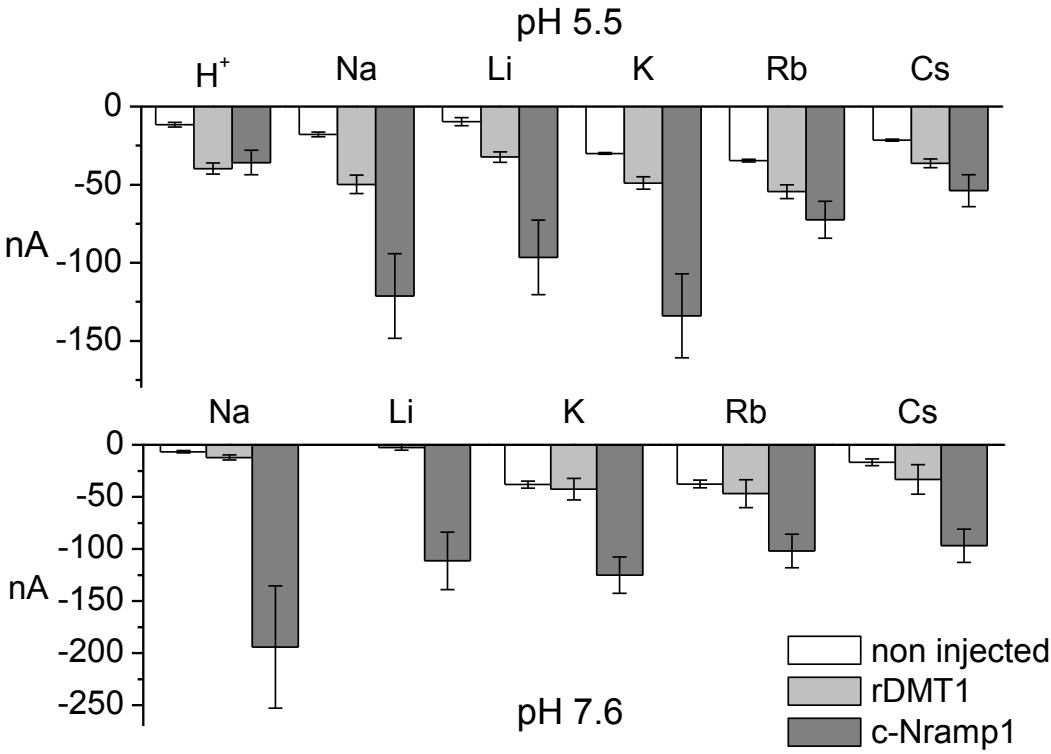

Figure 19. Mean leak current at pH 5.5 and pH 7.6. Histograms of the mean value of currents of non injected (white bars), *r*DMT1 expressing (light grey bars) or c-Nramp1(dark grey bars) expressing oocytes registered in the presence of different cationic solution at pH 5.5 (upper panel) or pH 7.6 (lower panel), at fixed voltage (V_h -40mV). The values were determined by subtraction of the value of the baseline (value of the current in the presence of TMA at pH 7.6) from the values recorded in the presence of different cations. Mean±SE of 5-16 oocytes derived from 2 batches.

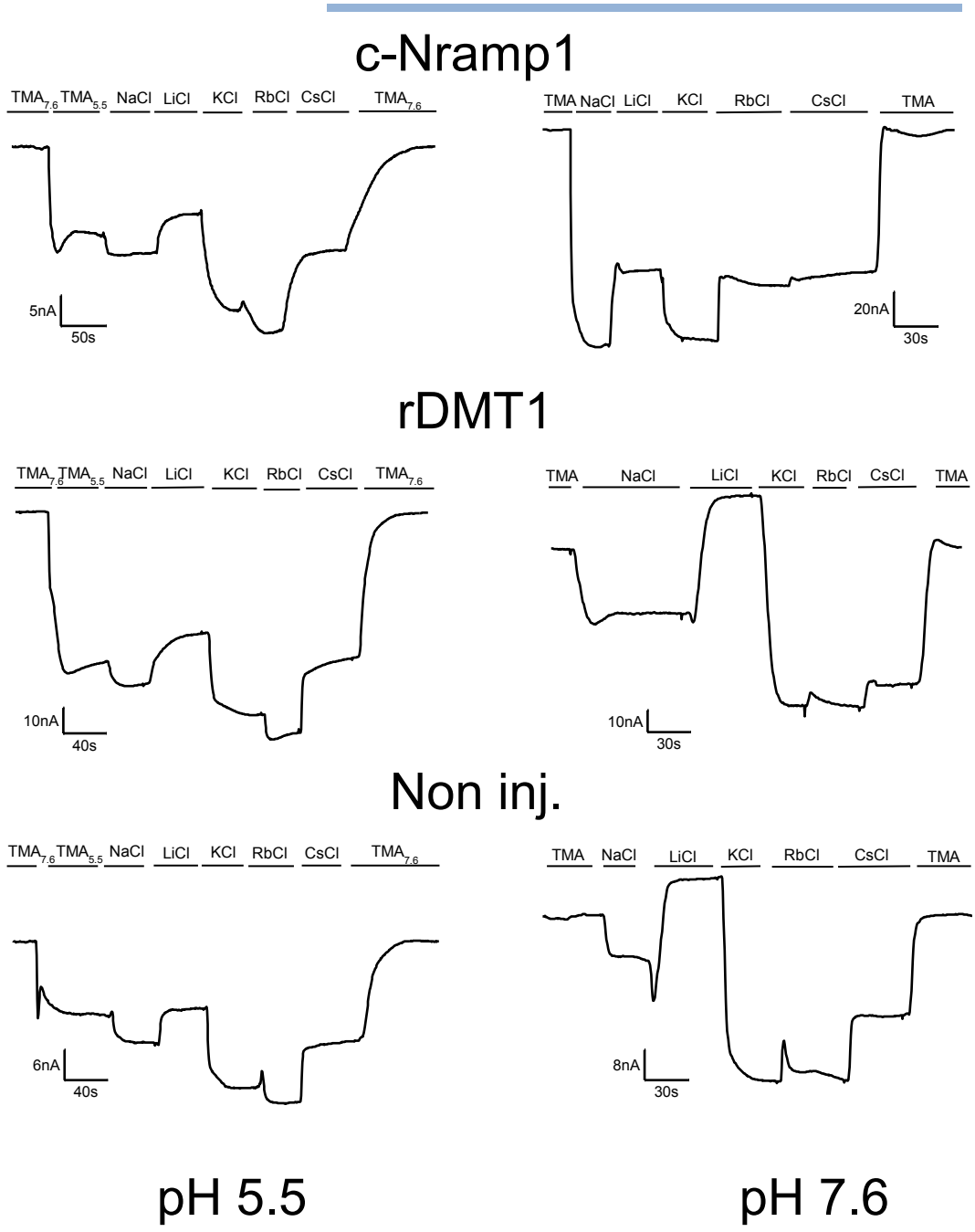

Figure 20. Representative traces of currents were recorded at pH 5.5 and 7.6 for non injected oocytes (control), *r*DMT1 and c-Nramp1 expressing oocytes respectively. Oocytes were clamped at a constant voltage of -40 mV and perfused with the indicated cations (TMA, sodium, lithium, potassium, rubidium, or cesium solution 98 mM).

The traces recorded at pH 5.5 and pH 7.6 were reported in Figure 20 for non injected oocytes (control), *r*DMT1 and c-Nramp1 expressing oocytes. All recording started with TMA at pH 7.6 considering this condition as "zero" currents for subsequent analysis of mean currents.

All the cationic solutions elicited current in all the oocytes tested; in c-Nramp1 oocytes at both pH generated currents with mean values of about 100nA (pH 5.5) and 200nA (pH 7.6) or even larger. The current amplitude in sodium solution at pH 7.6 was about 200 nA, and diminished as the pH decrease to 5.5. This behavior showed that sodium has a high permeability through the chimeric transporter. In lithium the currents were similar at both pH, an uncoupled current of -110 nA was present at pH 7.6 and reduced to -90 nA at pH 5.5. When the impermeant TMA solution was perfused, an inward current of about -30 nA was recorded at pH 5.5, showing that in the absence of other permeating cation the slippage of protons occurs. The same solutions and pH conditions tested in oocytes expressing *r*DMT1 showed an inward smaller (30 to 40 nA) current at pH 5.5 independently of the perfused solution; this is due to protons entering the transporter even in the absence of divalent metal ion, and showed the high specificity of the transporter for this substrate. At pH 7.6 the currents were similar to control oocyte, confirming that only proton can pass through *r*DMT1. In control oocytes, the acidic pH slightly depolarize the resting membrane potential. This is visualized in voltage clamp as an inward current of 2 to 5 nA. Since that *r*DMT1 didn't show leak current and that the two transporters displayed a different behavior for ion selectivity, we evaluated the peculiar ion specificity of c-Nramp1 considering the study of Eisenman sequence for equilibrium ion exchange [190], in order to verify if these leak currents were due to the transporter itself or to a channel conductance associated. Briefly, to discriminate between a channel (weak field strength site) and transporter (strong field strength site) must be considered hydratation energy and ion dimension. In the case of a transporter, ions can cross the membrane with their acqueous shell, and, on the other hand, in the case of a channel, ions diffuse quite freely, not associated with acqueous molecules, generating only weak interaction, but in a permeation pathway that require specific sites that mimic the hydration shell. Comparing the

Eisenman sequence for equilibrium ion exchange with c-Nramp1 selectivity let us classify it in the "X Eisenman sequence" where the order of the cation is $Na^+ > Li^+ > K^+ > Rb^+ > Cs^+$, the leak currents presented by the chimeric transporter were typical for a "strong interaction site" where ions pass through the transporter itself. On the contrary the low sequence number (III Eisenman sequence: $Rb^+ > K^+ > Cs^+ > Na^+ > Li^+$) of *r*DMT1 was not due to the transporter itself but to the endogenous channel proteins present on the oocyte membrane. In fact, in this transporter, not only the selectivity but also the current dimension were similar to control oocytes, where the currents recorded in the presence of different cations are surely due to their ion channels.

Dyctiostelium discoideum c-Nramp2 METAL TRANSPORTER: ELECTROPHYSIOLOGICAL CHARACTERIZATION

In contrast to c-Nramp1 and *r*DMT1, c-Nramp2 did not elicit any measurable transport current, either in sodium or in TMA solution, independently from substrates, holding potential, and pH of the testing solution (Figure 21). In addition, also in the presence of injected divalent metal ion inside the oocyte no currents were recorded. Consequently, it was necessary to verify the presence of c-Nramp2 on the membranes of the oocytes in order to verify the assumption that c-Nramp2 transporter could be electro-neutral.

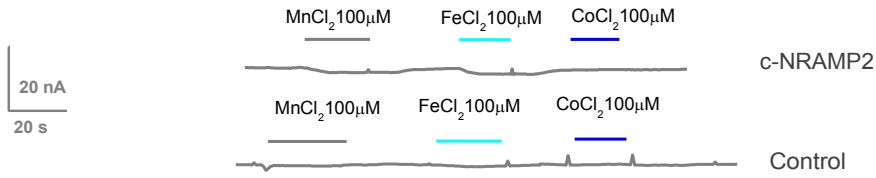

Figure 21. Transport associated current in c-Nramp2 expressing oocytes compared to control at a fixed potential (Vh -40mV). $MnCl_2$, $FeCl_2$ and $CoCl_2$ tested 100µM elicited transport associated currents similar to non injected oocytes.

IMMUNOLOCALIZATION EXPERIMENTS of c-Nramp1 AND c-Nramp2

Immunolocalization experiments on cryosections of oocytes were performed to evaluate the presence of the two chimeric proteins at the oocyte membrane. Oocytes expressing the transporters, as well non injected oocytes, were labeled with a rabbit primary polyclonal antisera anti-c-Nramp1 or c-Nramp2 and with a secondary antibody anti rabbit Cy3 conjugated.

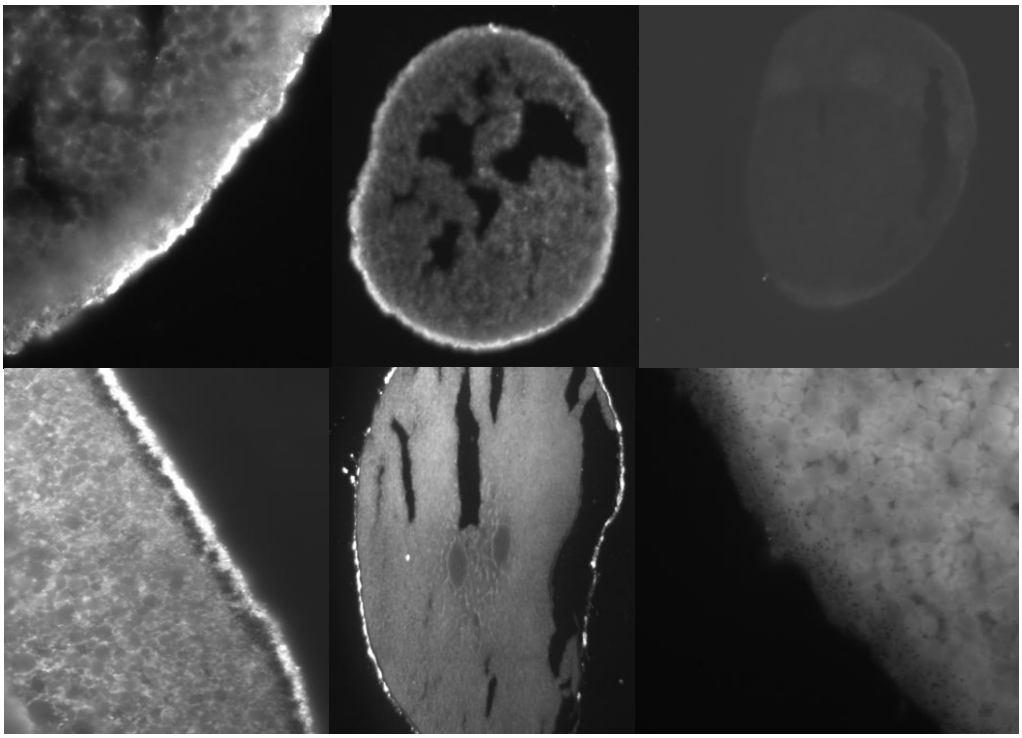

Figure 22. Immunolocalization of c-Nramp1 and c-Nramp2 on oocyte membrane. A- Immunolocalization experiments on oocytes expressing c-Nramp1; on the left 63x image, on the right 10x image; the last image is the control. **B-** Immunolocalization experiments on oocytes expressing c-Nramp2; on the left 63x image, on the right 10x image; the last image is the control. Experiments were repeated at least on five oocytes from two batches for each condition; controls are oocytes treated as samples but non injected with the cRNA of interest**.**

Representative images of immunocytochemical experiments are shown (Figure 22). The images, that were acquired with fluorescence microscopy (rhodamine filter set with λ excitation 550 and λ emission 580nm) confirmed the presence for c-Nramp1

and indicated that even c-Nramp2 transporter was well expressed on oocyte membranes.

MUTAGENIC STUDY ON c-Nramp2 TRANSPORTER

With the goal to find the electrogenic determinants of Nramp family, cNramp2 sequence was compared to different homologs, namely *r*DMT1, human Nramp2, *dd*Nramp1 and scaDMT. The choice of these homologs for the alignment is due to the newly described crystallography of scaDMT, to the mutation well described in literature of *r*DMT1 and *h*Nramp2 [126,178] and to the electrogenic activity of *dd*Nramp1 characterized in this thesis. The crystallography studies of Ehrnstorfer [139] showed that TMD1a, TMD1b, TMD6a and TMD6b transmembrane domains are involved in the interaction with the divalent metal substrates or with protons. Thus the alignment analysis suggest the creation of mutants of c-Nramp2 in order to obtain transporters with a clear electrogenic activity (Figure 23). These mutations were located in different but always crucial portion of the transporter. Site directed mutagenesis was then applied to create different c-Nramp2 mutants. In particular mutations involved in TMD1a were A119G and G125A; in TMD1b were A133E, the double mutant A133E/E137Q, E137Q, S140A, R141M; in TMD6a were T293V, the double mutant T299V/T300V; in TMD6b was F306Y.

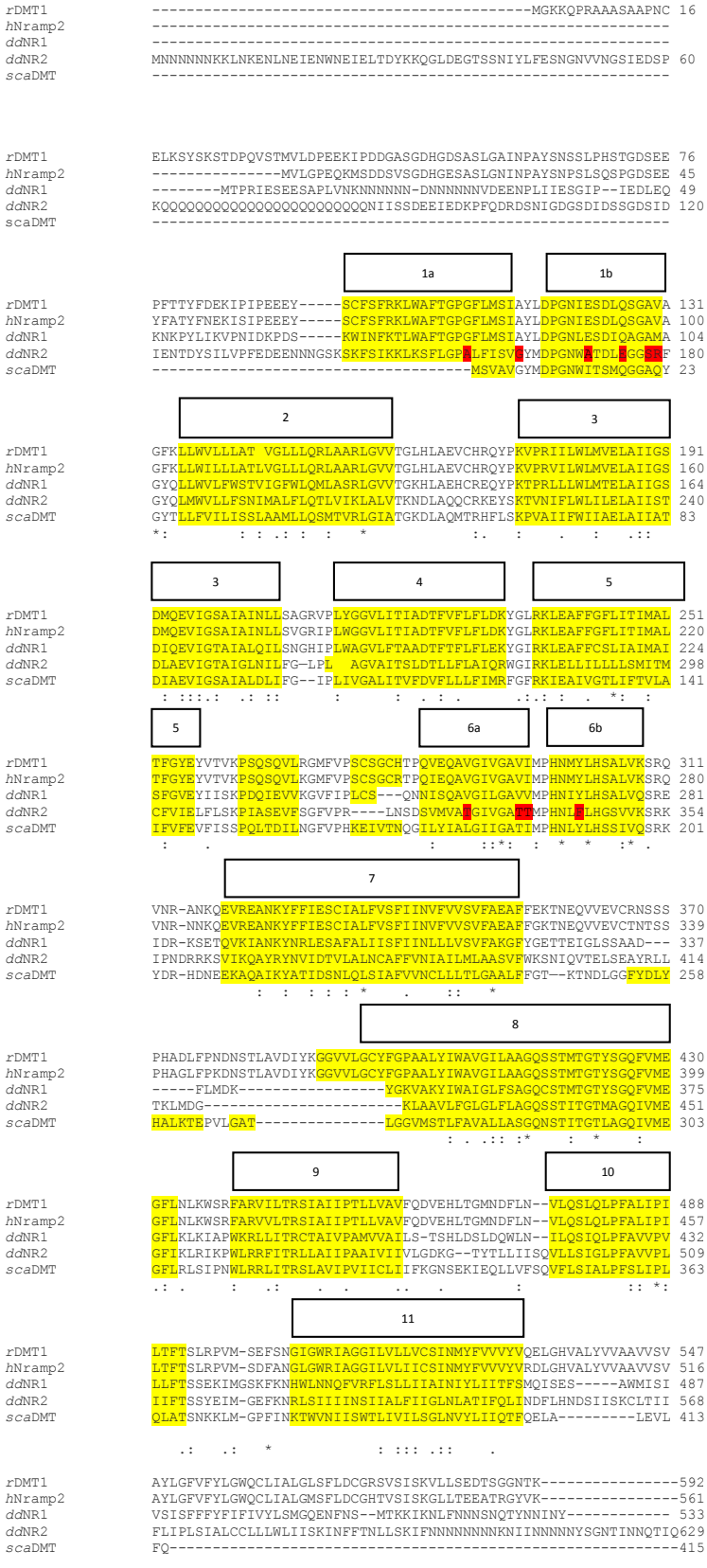

Figure 23. Alignment of different homologs of the SLC11 family. In yellow all the TMDs; in red on the sequence of *dd*Nramp2 the point mutations choosen to create all the mutants of c-Nramp2 wild type.

IMMUNOLOCALIZATION EXPERIMENTS of c-Nramp2 MUTANTS

Immunolocalization experiments on cryosections of oocytes were performed to evaluate whether the different c-Nramp2 mutants were localized or not on oocyte membrane. Oocytes expressing the transporters, as well non injected oocytes, were labeled with a rabbit primary polyclonal antisera anti-c-Nramp2 and with a secondary antibody anti rabbit Cy3 conjugated.

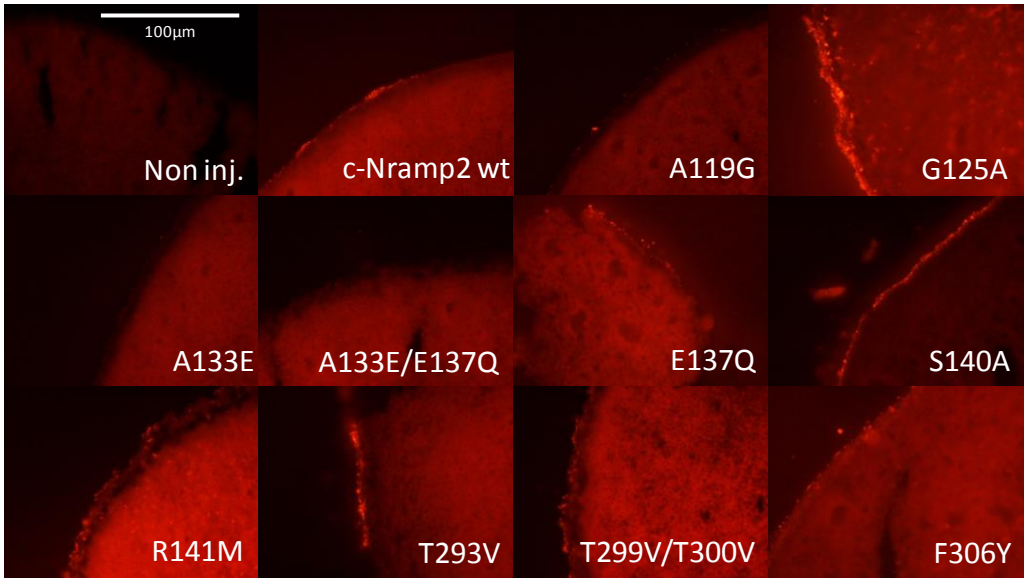

Figure 24. Immunolocalization of c-Nramp2 mutants on oocyte membrane. Immunolocalization experiments on oocytes expressing c-Nramp2 wt and all the c-Nramp2 mutants synthetized. In order: the negative control (non injected oocyte treated as samples but non injected with the cRNA of interest); c-Nramp2 wt and, in order of sequence all the c-Nramp2 mutants (A119G, G125A, A133E, A133E/E137Q, E137Q, S140A, R141M, T293V, T299V/T300V, F306Y). Experiments were repeated at least on five oocytes from different batches; all the images are 50x.

Representative images of immunocytochemical experiments are shown (Figure 24), non-injected oocytes were used as negative control but treated as sample. The images acquired with fluorescence microscopy (rhodamine filter set with λ excitation 550 and λ emission 580 nm) suggest that not all mutants seemed expressed on membrane. In particular A119G, A133E, the double mutant A133E/E137Q were not expressed at all; E137Q, R141M, the double mutant T299V/T300V, and F306Y were expressed at a lower extent; whereas G125A, S140A and T293V gave rise to an increased signal.

Given the overall results of immunocytochemistry we tried, despite the low expression, to perform electrophysiological experiments in order to verify the possible electrogenicity of c-Nramp2 mutants.

ELECTROPHYSIOLOGICAL CHARACTERIZATION of c-Nramp2 MUTANTS

All the mutants created, unfortunately, were not able to generate measurable transport associated currents, only the three mutants located in the TMD6 domains-namely T293V, the double mutant T299V/T300V and F306Y-elicited very small inward currents of 5-10 nA. Consequently, we developed a new method useful to study non electrogenic transporters.

DEVELOPMENT OF A NEW METHOD (XLO_S) TO DETERMINE FLUOROPHORE QUENCING IN OOCYTES

First the quantification by a microplate reader of the reduction in calcein fluorescence (quenching) in the presence of different concentration of divalent metal ions (Fe^{2+}, Mn^{2+} and Co^{2+}) was performed in order to verify the sensibility and the specificity of the fluorophore for the planned experiments (Figure 25).

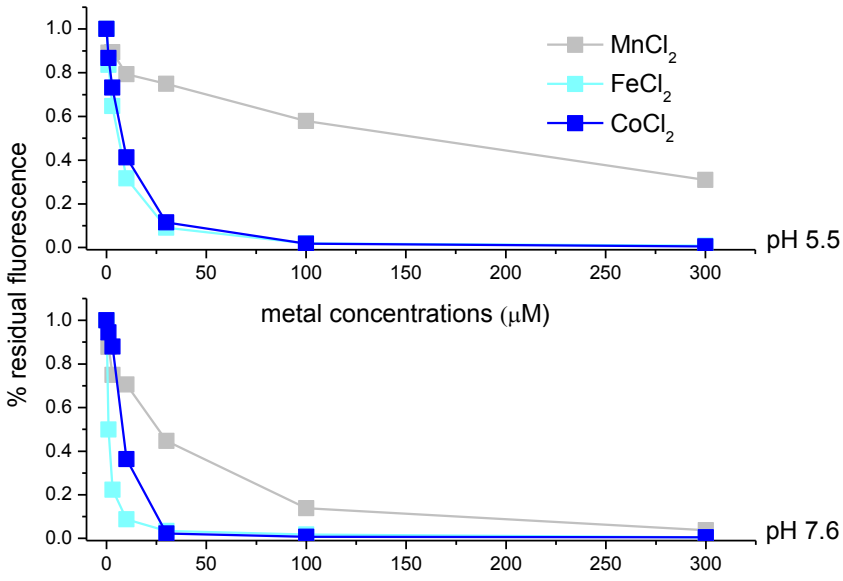

Figure 25. Dose response of calcein quenching at different pH. The results obtained with these three different metal ions confirmed that XLOs method is able to detect the residual fluorescence as other classical fluorescence technique.

The dose response experiments permit to determine at pH 5.5 and 7.6 the $K_{0.5}$ of the three main divalent metal transported by SLC11 family (Table 3) by the application of a logistic fitting (Origin 8.0).

$K_{0.5}$ pH 7.6		$K_{0.5}$ pH 5.5	
$K_{0.5}Mn^{2+}$	21±5.7µM	$K_{0.5}Mn^{2+}$	53.6+27µM
$K_{0.5}Fe^{2+}$	0.9±0.7µM	$K_{0.5}Fe^{2+}$	5.3+0.4µM
$K_{0.5}Co^{2+}$	9±3µM	$K_{0.5}Co^{2+}$	7.6+0.7µM

Table 3.$K_{0.5}$.

Each experimental condition tested with XLOs was also validated by comparison with traditional methods (uptake or TEVC) and confocal microscopy (Figure 26), measuring the calcein quenching directly on every single oocytes, confirming its efficacy.

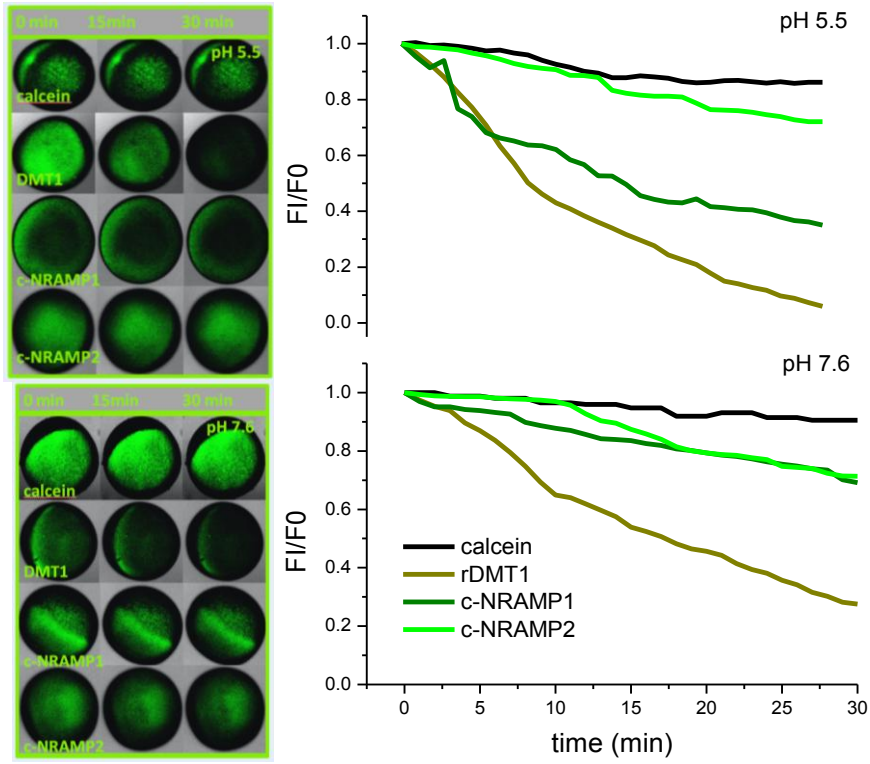

Figure 26. Confocal fluorescence quencing. The line "calcein" consider oocyte non expressing transporter, the divalent metal ion tested was $CoCl_2$ 100µM. The Δfluorescence was quantified with ratio FI/F0, where FI was the fluorescence intensity at different time, and F0 was the fluorescence at time 0. On the left of the figure, confocal series of images were taken at the time indicated, at the same condition.

Confocal microscopy experiments were conducted only with $CoCl_2$ that is not oxidizable, as $FeCl_2$, but with a $K_{0.5}$ similar, while $MnCl_2$ is quite less able to interact with calcein.

The quantification of the calcein fluorescence with XLOs in non injected oocytes or oocytes expressing the transporters in the absence of divalent metal ions were, as expected, comparable since that the fluorescence remain stable. Moreover in the presence or in the absence of transporter substrates ($MgCl_2$, $FeCl_2$ or $CoCl_2$), calcein fluorescence value in oocytes non expressing exogenous transporters was comparable, since that divalent metal ions were non-permeating in the absence of transport protein on the plasma membrane and consequently did not quench calcein inside the cell.

We performed XLOs experiment using a different fluorophore in order to confirm the general applicability of XLOs also with different transporters, not only SLC11 homologs. Dextran-FITC (Sigma) is pH sensitive, an acidification inside the oocyte quench the fluorophore. Due to this characteristic, we studied oocytes expressing Peptide transporter 1 (PepT1). This protein is a proton-coupled cotransporter (stoichiometry 1:1, peptide:proton). XLOs technique applied on oocytes expressing PepT1 provided results comparable to XLOs technique with calcein fluorophore and to traditional techniques (TEVC and confocal microscopy). The percentage of residual fluorescence in the presence of GQ 3mM in oocytes expressing PepT1 resulted statistically significant compared to controls (Figure 27); ($p<0.001$ with t-test vs non injected oocytes and vs oocytes expressing PepT1 in the absence of substrate; mean$\pm$SE of 105 oocytes, 7 batches).

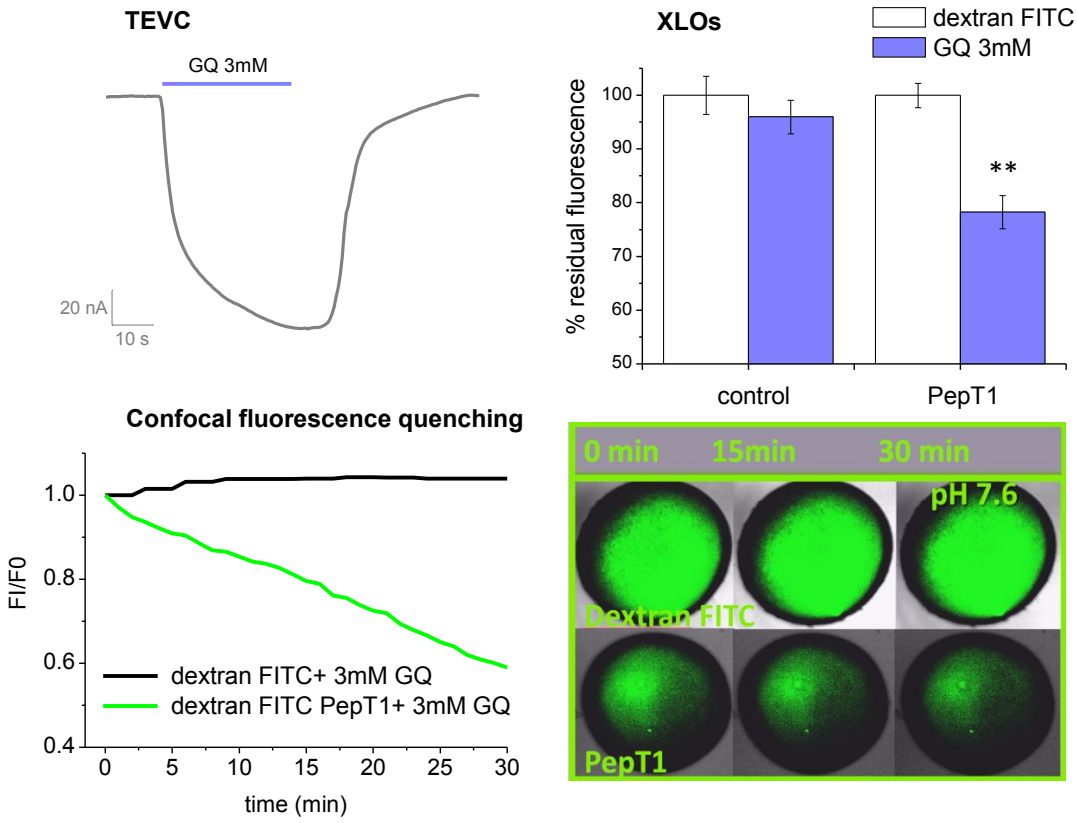

Figure 27. Dextran-FITC XLOs application. A. Transport associated current recorded with TEVC in PepT1 expressing oocytes at a fixed potential (V_h -60mV). GQ 3mM elicited huge transport associated current. **B**. Percentage of residual fluorescence measured with XLOs technique. Mean±SE of 105 oocytes, 7 batches ($p<0.001$ with t-test vs non injected oocytes and vs oocytes expressing PepT1 in the absence of substrate). Controls are oocytes non injected with cRNA of PepT1, in the absence or presence of GQ 3mM. **C**. Confocal fluorescence quencing. The black line represents non injected oocyte. The green line represents oocytes expressing PepT1.The fluorescence variation over time were quantified with ratio FI/F0, FI was the fluorescence intensity at different time, F0 was the fluorescence at time 0. **D**. Confocal images were taken at the time indicated at the same condition.

All together these preliminary experiments demonstrated the validity, sensibility and specificity of XLOs method and support our future results on metal ion transporters studied with this new technique.

DETERMINATION OF TRANSPORT ACTIVITY IN OOCYTES EXPRESSING WILD TYPE METAL TRANSPORTER BY FLUOROPHORE QUENCING

We introduced a new method to detect the uptake of the substrate by monitoring the changes in calcein fluorescence due to ion metal interaction with the fluorophore.

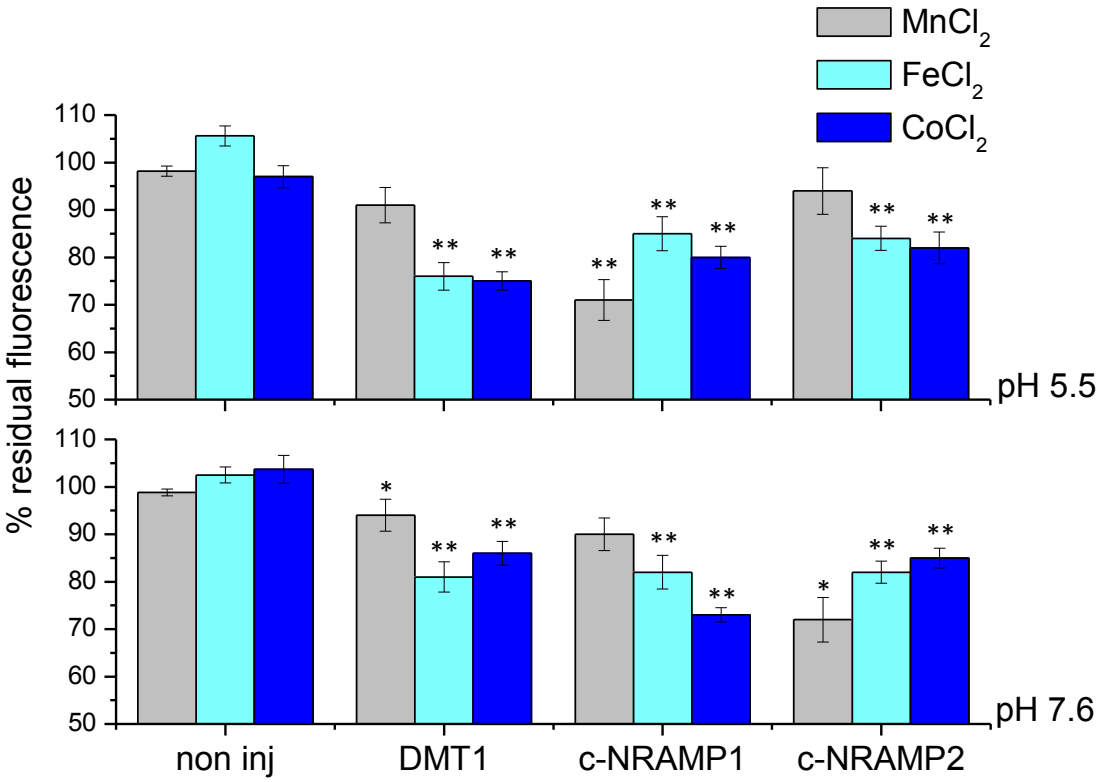

Figure 28. Percentage of residual fluorescence measured with XLOs. Data were reported as percentage of residual fluorescence compared to control (non injected oocytes in the absence of substrates, fixed at 100%). **p<0.001, *p<0.05 t-test, all transporters vs controls tested with the same divalent metal ion at different pH (5.5 and 7.6). Histograms are mean±SE of 75-150 oocytes, 5-10 batches.

Oocytes expressing different metal transporters were microinjected with calcein, incubated with different solutions of divalent metals for one hour, and the resulting fluorescence quenching was quantified by microplate reader. XLOs was used to test divalent metal ion transport in *r*DMT1, c-Nramp1, c-Nramp2 expressing oocytes using calcein as fluorescence indicator and $MnCl_2$, $FeCl_2$ and $CoCl_2$ as substrates. The

quenching action of metals entered in the oocytes by selected SLC11 transporters was statistically significant if compared to the quenching results obtained in non injected oocytes (Figure 28; **p<0.001; *p<0.05 t-test).

All the residual fluorescence obtained were calculated as percentage of residual fluorescence compared to control (non injected oocytes in the absence of substrates considered 100%). In particular in oocytes expressing *r*DMT1, Fe^{2+} and Co^{2+} induced a similar quenching of 75% at pH 5.5 and to a lesser extent also Mn^{2+} (Co^{2+} >Fe^{2+} >Mn^{2+}). At pH 7.6 the metal ions ability to quench the fluorophore was lower to that at pH 5.5 (80-85% of residual fluorescence) and with a different capacity between ions to quench calcein (Fe^{2+}>Co^{2+}>Mn^{2+}). This data confirmed the electrophysiological experiments on that transporter. c-Nramp1 expressing oocytes showed that Mn^{2+} (73% of residual fluorescence), Co^{2+}(80% of residual fluorescence) and Fe^{2+} (85% of residual fluorescence) at pH 5.5 were transported and were able to quench calcein with ion selectivity: Mn^{2+}>Fe^{2+} >Co^{2+}. At pH 7.6 c-Nramp1 transported Co^{2+}>Fe^{2+}>Mn^{2+} ranging from a residual fluorescence of 75% for Co^{2+} to 90% for Mn^{2+}.

Moreover, with this technique we obtained information about c-Nramp2 transporter, expressed accordingly to immunocytochemistry results, but not electrogenic. c-Nramp2 expressing oocytes showed that Fe^{2+} and Co^{2+}(82% of residual fluorescence) were transported and were able to quench calcein whereas the transport of Mn^{2+} was very low (94% of residual fluorescence), showing the ion selectivity: Co^{2+}>Fe^{2+}>Mn^{2+} with the last with a poor efficacy to quench calcein at pH 5.5. At neutral pH the transporter displayed a different ion selectivity: Mn^{2+} (72% of residual fluorescence)>Fe^{2+} (82% of residual fluorescence)>Co^{2+} (85% of residual fluorescence). At pH 7.6 c-Nramp2 transported divalent metal ions better than at pH 5.5. These data obtained were significant for all transporters studied compared to controls tested with the same divalent metal ions at different pH (5.5 and 7.6), with the exception for the data of Mn^{2+} transported by c-Nramp1 at pH 7.6 and Mn^{2+} transported by c-Nramp2 at pH 5.5, that were not significantly different from controls.

DETERMINATION OF TRANSPORT ACTIVITY IN MUTANTS OF c-NRAMP2 OOCYTES BY FLUOROPHORE QUENCING

The method XLOs, that we applied to characterize the transporter c-Nramp2 wild type, permitted also the analysis of c-Nramp2 mutants. Their expression on oocyte membrane were demonstrated with immunological experiments and also with electrophysiological experiments, although on T293V, T299V/T300V and F306Y only. The low level of expression of c-Nramp2 wild type and of all c-Nramp2 mutants led us to perform anyway the XLOs experiments on all mutants, testing also those that seemed not present on oocyte membrane with immunolocalization experiments.

c-Nramp2 mutant	% residual fluorescence pH 5.5	% residual fluorescence pH 7.6
A119G	84% (100% of WT)	83% (101% of WT)
G125A	91% (108% of WT)	94% (115% of WT)
A133E	83% (99% of WT)	86% (105% of WT)
E137Q	85% (101%of WT)	83% (101%of WT)
A133E/E137Q	81% (96%of WT)	87% (106% of WT)
S140A	79% (94% of WT)	83% (101%of WT)
R141M	90% (107% of WT)	87% (106% of WT)
T293V	88% (105% of WT)	73% (89% of WT)
T299V/T300V	65% (77% of WT)	73% (89% of WT)
F306Y	80% (95% of WT)	78% (95% of WT)
c-Nramp2 wild type	84%	82%

Table 4. XLOs c-Nramp2 mutants. The percentages described in the table are mean of 2-4 batches, 15 oocytes utilized in every condition tested. In parenthesis the quenching related to c-Nramp2 wild type considered 100%. In light blue were evidenced the mutants where the residual fluorescence were lower compared to c-Nramp2 wild type. In grey were evidenced the mutants that immunolocalization experiments considered not expressed on oocytes membrane.

We analyzed the uptake activity with XLOs technique in all of them with the aim to obtain data also on electroneutral ones, since that their presence on oocytes membrane was already demonstrated with immunolocalization experiments. Oocytes expressing different c-Nramp2 mutants, c-Nramp2 wild type or control oocytes were microinjected with calcein, incubated in the presence of $FeCl_2$ 100μM at different pH condition (5.5 and 7.6) for one hour, and the resulting fluorescence quenching was quantified by a microplate reader. The results were analyzed comparing the percentage of residual fluorescence of all the mutants to c-Nramp2 wild type (Table 4). The residual fluorescence obtained with T293V, T299V/T300V and F306Y suggested that these three mutants were more functional compared to c-Nramp2, although the inward currents generated were still little.

A119G, A133E and the double mutant A133E/E137Q seemed not expressed on membrane and neither functional.E137Q and R141M seemed expressed on membrane at a lower extent but similar to c-Nramp2 wild type for their functionality. The last two mutants, G125A and S140A, were well expressed on oocytes membrane but G125A seemed non functional and S140A with a functionality comparable to c-Nramp2 wild type.

DISCUSSION

Iron is an element necessary for all the organisms; its role in essential metabolism, cellular processes, energy production, biosynthesis is fundamental for life of unicellular organism to human. Although being so important, it has harmful properties in its free form, in order to neutralize those negative effects, iron need to be linked to proteins in the cell. Iron homeostasis is finely regulated at different level and with different cells as protagonists: enterocytes absorb iron from food, macrophages recycle iron derived from erythrocytes destruction, hepatocytes are the principal storage of iron. An imbalance in regulation of iron homeostasis will cause different pathologies where iron play a role, for its rise causing iron overload disorders or for its reduction giving rise to iron deficiency pathologies [1]. Studies on iron homeostasis, regulation and transport could be also done with a simplified model of professional phagocyte and pathogen host, *Dyctiostelium discoideum (Dd)*. *Dd* is a model organism for studying how host resists to infection or the pathogen escape defense strategies [108]. Iron homeostasis is fundamental for the resistance to pathogen bacteria in higher eukaryotes as in *Dd*. In mammals like in *Dd* many genes regulate iron homeostasis. Among these, genes of SLC11 family, in mammals as in *Dd*, codify for iron transporters. In mammals, Nramp1 (SLC11A1) expression is limited to the lysosomal membrane of mature macrophages, granulocytes and monocytes [130]. *Dd* Nramp1, like mammalian ortholog, is expressed only in phagosomes and macropinosomes. Nramp1 is a symporter H^+/divalent metal ions out the lysosome; this action removes iron and other metals fundamental for intracellular pathogens [131]. Another metal transporter-Nramp2 (SLC11A2, or DMT1)-is present on plasma membrane of several tissues; mutations in the mammal Nramp2 transporter are associated to severe microcytic anemia, serum and hepatic iron overload [126,132]. In *Dd*, Nramp2 is localized as membrane protein in the contractile vacuole, which regulates osmolarity. The presence in different compartments of Nramp1 and Nramp2 suggests that both transporters jointly play a role in iron homeostasis.

Our findings about the function of c-Nramp1 and c-Nramp2, in particular, their role in divalent metals transport add new insights concerning the mechanism of action of these proteins and their mammalian ortholog.

For the characterization of the the iron transporters of *Dictyostelium discoideum*, *dd*Nramp1 and *dd*Nramp2 has been expressed in *X. laevis* oocytes. These original proteins *dd*Nramp1 and *dd*Nramp2 had a very low level of expression, probably because these two transporters are not plasma membrane proteins in the social amoeba. *dd*Nramp1 and *dd*Nramp2 tested by electrophysiology did not elicit currents of sufficient amplitude to characterize the functionality of these transporters. Consequently the synthesis of chimeric proteins, where N and C-termini of both proteins were replaced with the N- and C-termini of *r*DMT1, was done to increase their expression on the plasma membrane and allowing the functional characterization of both transporters. Before starting with the functional studies, we performed an analysis of the evolutionary distance between *D. discoideum* and *X. laevis*, looking for the differences in the codon usage between these two organisms. The codon usage analysis predicted problems in the protein synthesis by *X. laevis* oocytes, due to the utilization of rare codons in the original sequence, the rare codon usage in c-Nramp2 was even higher than for c-Nramp1.

The characterization of the c-Nramp1 metal transporter by classical electrophysiological recordings, demonstrated the specificity of this transporter for divalent transition metals, with maximal inward currents at acidic pH in the presence of iron and manganese, confirming the SLC11 family features. $FeCl_2$ and $MnCl_2$ were able to elicit inward transport currents also at low concentrations suggesting the high affinity of the transporter for these ions. The analysis of the ion dependence showed transport currents in the presence of both Na and TMA, indicating c-Nramp1 as a sodium independent transporter. The different behavior at neutral pH in the presence of substrates when Na or TMA are used as driving ions allowed to observe the presence of the sodium leak current. This particular current of c-Nramp1present only in sodium solution was also detected in the yeast Smf1p transporter [187,188]. This sodium leak current is due to the access through c-Nramp1 in an uncoupled way of the sodium ions and give raise to a huge current that diminished drastically in the presence of substrates and protons, i.e. when the transporter switches in the “transporter mode”. This peculiar sodium leak current is present mainly at neutral pH, whereas the competition for the binding site with protons at higher concentration-at acidic pH- reduces its amplitude.

This permeation property was compared with *r*DMT1. This latter didn't show leak current and the two transporters displayed a different behavior for ion selectivity in the absence of substrate. We compared the peculiar ion specificity of c-Nramp1 with the Eisenman sequence for equilibrium ion exchange [190], in order to verify if leak currents were due to the transporter itself or to a channel conductance associated. c-Nramp1 ion preferences in the absence of substrate can be classified in the "X Eisenman sequence" where the order of the cation is $Na^+ > Li^+ > K^+ > Rb^+ > Cs^+$, distinctive of a "strong interaction site" where ions can be consider to pass through the transporter itself. On the contrary the low sequence number (III Eisenman sequence: $Rb^+ > K^+ > Cs^+ > Na^+ > Li^+$) identified for controls (non injected oocytes) and also for *r*DMT1 is typical for a channel like permeation. The absence of leak current and the behavior similar to control oocytes, that normally do not express at high level any transporter, but only some endogenous channels (especially potassium channels), suggest that the sequence of currents recorded in *r*DMT1 expressing oocytes was not due to the transporter itself but to endogenous channel proteins of the oocyte membrane.

Electrophysiological experiments on c-Nramp2, given the higher predicted difficulty on oocytes expression suggested by codon usage analysis, conducted us to verify the presence of c-Nramp2 on oocytes membranes. Immunolocalization experiments confirmed the presence of both the transporters on membrane of expressing oocytes. The presence on the plasma membrane, even of c-Nramp2, strongly encouraged the assumption that this transporter is electro-neutral.

With the goal to find the electrogenic determinants of Nramp family, c-Nramp2 sequence was compared to different homologs. Alignment analysis in order to evaluate the degree of conservation of *dd*Nramp1, *dd*Nramp2 with mammalian *h*Nramp2 and *r*DMT1. The analysis showed a high degree of conservation, with some interesting differences, which can be evidenced by comparing these proteins with the prokaryotic ScaDMT, recently crystallized as model of the SLC11 family [139]. Crystallography and functional topology studies [191] show that two symmetrically oriented helics in the center of the membrane bilayer, formed by the second half of the first transmembrana α-helix are face-to-face with a symmetric half of the sixth α-helix,

resulting in the formation of the ion channel and of the substrate-binding site. Different residues, fundamental for ion binding and proton co-transport were present in the TMD1a, TMD1b, TMD6a and TMD6b, were conserved in all the proteins aligned, mammalian Nramp proteins, scaDMT as well as *Dyctiostelium* counterparts. Literature analysis looking for mutations able to affect uptake, substrate specificity, pH dependence of transport or leak current [126,133,178,181,185], indicated that only one of this site is different between *dd*Nramp1 (C116) and *h*Nramp2 (G208), whereas three residues were different in *dd*Nramp2 (A171, E175 and L290) corresponding to E87, Q91, G208 in *h*Nramp2. Interestingly, the equivalent mutations E87A, Q91D and G208R in *r*DMT1 result in decreased metal uptake in *Xenopus laevis* oocytes [133]. All these aminoacidic differences could justify results obtained with c-Nramp2, and its probable electroneutrality. Therefore we decided to insert mutation in c-Nramp2 in order to obtain a protein more similar to *dd*Nramp1 and to other homologs, with the goal to restore the electrogenicity. Site directed mutagenesis was then applied to create c-Nramp2 mutants. In particular mutations localized in TMD1a were A119G and G125A; in TMD1b were A133E, the double mutant A133E/E137Q, E137Q, S140A, R141M; in TMD6a were T293V, the double mutant T299V/T300V; in TMD6b was F306Y.

The presence of the mutants on oocytes membrane was verified by immunocytochemical experiments. We performed immunolocalization experiments with a custom primary antibody polyclonal that could be not able to detect lowest protein expression; results should be underestimated. In fact, images suggested that not all mutants were well expressed on membrane. In particular A119G, A133E, the double mutant A133E/E137Q were apparently not expressed at all; E137Q, R141M, the double mutant T299V/T300V, and F306Y were expressed at a lower extent; whereas G125A, S140A and T293V gave rise to an increased signal. On the same c-Nramp2 mutants, despite the low expression or even the apparent lack of expression, we performed-anyway-electrophysiological experiments to verify the possible electrogenicity of c-Nramp2 mutants synthetized. Unfortunately, only the three mutants located in the TMD6 domains elicited very small inward currents. This

electrophysiological data suggested that these mutations in TMD6 slightly change c-Nramp2 wild type behavior.

All these results underlined the necessity of a different approach to study transporters that are electro-neutral. We developed a new assay, named XLOs, which could be utilized in substitution to well establish radiolabeled uptake assays. Our novel assay is based on calcein (a metal indicator fluorophore) injection into the oocyte and quantification of its quenching, as a consequence of imported divalent metals, in every single oocyte.

Each experimental condition tested with XLOs was also validated by comparison with traditional methods (uptake, TEVC) and confocal microscopy. XLOs was used to verify divalent metal ion transport in *r*DMT1, c-Nramp1, c-Nramp2 expressing oocytes using calcein as fluorescence indicator and $MnCl_2$, $FeCl_2$ and $CoCl_2$ as substrates. We demonstrated that the quenching action of metals entered in the oocytes by SLC11 transporters was statistically significant if compared to the results obtained in non injected oocytes. The data obtained with *r*DMT1 with the application of XLOs confirmed the electrophysiological experiments on that transporter; the metal ions ability to quench the fluorophore was higher at pH 5.5 (80-85% of residual fluorescence) and displayed a different capacity between ions to quench calcein (Fe^{2+}>Co^{2+}>Mn^{2+}). Regarding c-Nramp1 expressing oocytes, Mn^{2+} (73% of residual fluorescence), Co^{2+}(80% of residual fluorescence) and Fe^{2+} (85% of residual fluorescence) at pH 5.5 were transported and able to quench calcein with ion selectivity: Mn^{2+}>Fe^{2+} >Co^{2+}. At pH 7.6 the transport was still present, obtaining similar percentages of residual fluorescence although with a different ion selectivity.

c-Nramp2 expressing oocytes showed that Fe^{2+} and Co^{2+} were transported and were able to quench calcein whereas the transport of Mn^{2+} was very low, with the last that has a poor efficacy to quench calcein at pH 5.5. At neutral pH c-Nramp2 transported divalent metal ions better than at pH 5.5 and displayed a different ion selectivity: Mn^{2+}>Fe^{2+}>Co^{2+}.

Until 2016, only two works has been published on the characterization of metal transporters in Xenopus oocytes with fluorescent probes, namely to investigate DMT1 transport using Phen Green SK [192] and our work where the fluorophore was studied

with confocal microscopy in oocytes expressing c-Nramp1, c-Nramp2 and *r*DMT1 [193]. All these differences between the two *D. discoideum* transporters, namely *dd*Nramp1 and *dd*Nramp2, should be due not only to structural differences but also to the less efficient c-Nramp2 expression in *X. laevis* oocytes.

c-Nramp2 mutants expression on oocyte membrane were demonstrated with immunolocalization experiments and also with electrophysiological experiments. The low level of expression of c-Nramp2 wild type and of all c-Nramp2 mutants suggested us to perform XLOs experiments on all mutants, also on those that seemed not present on oocyte membrane. The data obtained, together with our previous immunological and electrophysiological informations, permitted us to characterize the mutants of c-Nramp2. In particular, the mutants T293V, T299V/T300V and F306Y, located on TMD6, were the only three mutants more functional than c-Nramp2 wild type not only considering transport inward currents, but also with XLOs analysis of the residual fluorescence. A119G, A133E and the double mutant A133E/E137Q seemed not expressed on membrane and neither functional, probably the aminoacidic substitution of alanine and glutamic acid to glutamic acid and glutamine, respectively, changed the charge distribution of the protein influencing structure and function. E137Q and R141M seemed expressed on membrane at a lower extent but similar to c-Nramp2 wild type for their functionality. The last two mutants, G125A and S140A, were well expressed on oocytes membrane but G125A seemed non functional and S140A with a functionality comparable to c-Nramp2 wild type.

Our data on XLOs, based on fluorophore quenching followed by microplate reader analysis, permit us to obtain results from tens of oocytes in different experimental condition at the same time, achieving significant statistical data from the same batch saving time and animals. In particular, let us to collect data on electro-neutral transporters, not suitable to be studied with the classical electrophysiology.

Data on purified phagosomes of Dictyostelium cells, demonstrated that Nramp1 was essential for iron transport, which was imported into the phagosomes at a slightly acidic pH if a source of ATP was provided to activate the V-H^+-ATPase [115]. Moreover Nramp1 is also essential *in vivo* where mediates iron efflux from macropinosomes to the cytosol, thus confirming that Nramp1 promote iron depletion

from phagosomes [193]. Phagocytosis is fundamental for Dictyostelium cells to engulf bacteria, their nutritional source, but also potential pathogenic bacteria [108,193]. Dictyostelium Nramp1 displays, therefore, both a nutritive and a protective function, favoring accumulation of iron in the cytoplasm upon bacterial digestion and simultaneously depriving pathogenic bacteria relegated in phagosomes or macropinosomes from an essential element. This peculiar dual role is similar to that of the Nramp1 ortholog in mammals macrophages, which recycles iron from ingested erythrocytes, while starving ingested pathogens from iron or manganese [135,174].

In conclusion, XLOs application permitted also the characterization of *dd*Nramp2. The site directed mutagenesis studies helped us to clarify the mechanism of action of *dd*Nramp2, suggesting new insights for the study on iron transport across the contractile vacuole membrane, where *dd*Nramp2 is expressed, and the function of this organelle in the homeostasis of divalent metal in *D. discoideum*, the animal model for phagocytosis and immunological study.

REFERENCES

1. Silva B, Faustino P. An overview of molecular basis of iron metabolism regulation and the associated pathologies. Biochim Biophys Acta 2015;1852(7):1347-1359.
2. Miller DD, Berner LA. Is solubility in vitro a reliable predictor of iron bioavailability? Biol Trace Elem Res 1989;19:11-24.
3. Walling C, Partch RE, Weil T. Kinetics of the decomposition of hydrogen peroxide catalyzed by ferric ethylenediaminetetraacetate complex. Proc Natl Acad Sci USA 1975;72:140-142.
4. Park CH, Bacon BR, Brittenham GM, Tavill AS. Pathology of dietary carbonyl iron overload in rats. Lab Invest 1987;57:555-563.
5. Charlton RW, Bothwell TH. Iron absorption. Annu Rev Med 1983;34:55-68.
6. Ganz T. Hepcidin-a regulator of intestinal iron absorption and iron recycling by macrophages. Best Pract Res Clin Haematol 2005;18:171-182.
7. Sharp PA. Intestinal iron absorption: regulation by dietary & systemic factors. Int J Vitam Nutr Res 2010;80:231-242.
8. Laftah AH, Latunde-Dada GO, Fakih S et al. Haem and folate transport by proton-coupled folate transporter/haem carrier protein 1 (SLC46A1). Br J Nutr 2009;101:1150-1156.
9. McKie AT, Barrow D, Latunde-Dada GO et al. An iron-regulated ferric reductase associated with the absorption of dietary iron. Science 2001;291:1755-1759.
10. Ohgami RS, Campagna DR, McDonald A, Fleming MD. The Steap proteins are metalloreductases. Blood 2006;108:1388-1394.
11. Gunshin H, Mackenzie B, Berger UV et al. Cloning and characterization of a mammalian proton-coupled metal-ion transporter. Nature 1997;388:482-488.
12. Galy B, Ferring-Appel D, Becker C et al. Iron regulatory proteins control a mucosal block to intestinal iron absorption. Cell Rep 2013;3:844-857.
13. Le NT, Richardson DR. Ferroportin1: a new iron export molecule? Int J Biochem Cell Biol 2002;34:103-108.

14. Yeh KY, Yeh M, Mims L, Glass J. Iron feeding induces ferroportin 1 and hephaestin migration and interaction in rat duodenal epithelium. Am J Physiol Gastrointest Liver Physiol 2009;296:G55-G65.
15. Brittin GM, Chee QT. Relation of ferroxidase (ceruloplasmin) to iron absorption. J Lab Clin Med 1969;74:53-59.
16. Young S, Bomford A. Transferrin and cellular iron exchange. Clin Sci (Lond) 1964;67:273-278.
17. Brown PJ, Johnson PM. Isolation of a transferrin receptor structure from sodium deoxycholate-solubilized human placental syncytiotrophoblast plasma membrane. Placenta 1981;2:1-10.
18. Fleming MD, Romano MA, Su MA et al. Nramp2 is mutated in the anemic Belgrade (b) rat: evidence of a role for Nramp2 in endosomal iron transport. Proc Natl Acad Sci USA 1998;95:1148-1153.
19. Hershko C, Graham G, Bates GW, Rachmilewitz EA. Non-specific serum iron in thalassaemia: an abnormal serum iron fraction of potential toxicity. Br J Haematol 1978;40:255-263.
20. Grootveld M, Bell JD, Halliwell B et al. Non-transferrin bound iron in plasma or serum from patients with idiopathic hemochromatosis. Characterization by high performance liquid chromatography and nuclear magnetic resonance spectroscopy. J Biol Chem 1989;264:4417-4422.
21. Liuzzi JP, Aydemir F, Nam H et al. Zip14 (Slc39a14) mediates non-transferrin-bound iron uptake into cells. Proc Natl Acad Sci USA 2006;103:13612-13617.
22. Andrews A. Disorders of iron metabolism. N Engl J Med 2000;342:1293 (author reply 1294).
23. Shi H, Bencze KZ, Stemmler TL, Philpott CC. A cytosolic iron chaperone that delivers iron to ferritin. Science 2008;320:1207-1210.
24. Sheftel AD, Zhang AS, Brown C et al. Direct interorganellar transfer of iron from endosome to mitochondrion. Blood 2007;110:125-132.

25. Liu X, Theil EC. Ferritin as an iron concentrator and chelator target. Ann N Y Acad Sci 2005;1054:136-140.
26. Levi S, Corsi B, Bosisio M et al. A human mitochondrial ferritin encoded by an intronless gene. J Biol Chem 2001;276:24437-24440.
27. Larson JA, Howie HL, So M. Neisseria meningitidis accelerates ferritin degradation in host epithelial cells to yield an essential iron source. Mol Microbiol 2004;53:807-820.
28. Mehlhase J, Sandig G, Pantopoulos K, Grune T. Oxidation-induced ferritin turnover in microglial cells: role of proteasome. Free Radic Biol Med 2005;38:276-285.
29. Mancias JD, Wang X, Gygi SP et al. Quantitative proteomics identifies NCOA4 as the cargo receptor mediating ferritinophagy. Nature 2014;509:105-109.
30. Nilsson R, Schultz IJ, Pierce EL et al. Discovery of genes essential for heme biosynthesis through large-scale gene expression analysis. Cell Metab 2009;10:119-130.
31. Dowdle WE, Nyfeler B, Nagel J et al. Selective VPS34 inhibitor blocks autophagy and uncovers a role for NCOA4 in ferritin degradation and iron homeostasis in vivo. Nat Cell Biol 2014;16:1069-1079.
32. Pollard JW. Trophic macrophages in development and disease. Nat Rev Immunol 2009;9:259-270.
33. Low PS, Waugh SM, Zinke K,. Drenckhahn D. The role of hemoglobin denaturation and band 3 clustering in red blood cell aging. Science 1985;227:531-533.
34. Pantaleo A, Giribaldi G, Mannu F et al. Naturally occurring anti-band 3 antibodies and red blood cell removal under physiological and pathological conditions. Autoimmun Rev 2008;7:457-462.
35. Lee SJ, Park SY, Jung MY et al. Mechanism for phosphatidylserine dependent erythrophagocytosis in mouse liver. Blood 2011;117:5215-5223.

36. Bosman GJ, Willekens FL, Werre JM. Erythrocyte aging: a more than superficial resemblance to apoptosis? Cell Physiol Biochem 2005;16:1-8.
37. Poss KD, Tonegawa S. Heme oxygenase 1 is required for mammalian iron reutilization. Proc Natl Acad Sci USA 1997;94:10919-10924.
38. Kristiansen M, Graversen JH, Jacobsen C et al. Identification of the haemoglobin scavenger receptor. Nature 2001;409:198-201.
39. Soe-Lin S, Apte SS, Andriopoulos Jr B et al. Nramp1 promotes efficient macrophage recycling of iron following erythrophagocytosis in vivo. Proc Natl Acad Sci USA 2009;106:5960-5965.
40. Harris ZL, Durley AP, Man TK, Gitlin JD. Targeted gene disruption reveals an essential role for ceruloplasmin in cellular iron efflux. Proc Natl Acad Sci USA 1999;96:10812-10817.
41. Finch C. Regulators of iron balance in humans. Blood 1994;84:1697-1702.
42. Gavin MW, McCarthy DM, Garry PJ. Evidence that iron stores regulate iron absorption-a set point theory. Am J Clin Nutr 1994;59:1376-1380.
43. Nicolas G, Bennoun M, Devaux I et al. Lack of hepcidin gene expression and severe tissue iron overload in upstream stimulatory factor 2 (USF2) knockout mice. Proc Natl Acad Sci USA 2001;98:8780-8785.
44. Lin L, Valore EV, Nemeth E et al. Iron transferring regulates hepcidin synthesis in primary hepatocyte culture through hemojuvelin and BMP2/4. Blood 2007;110:2182-2189.
45. Nicolas G, Chauvet C, Viatte L et al. The gene encoding the iron regulatory peptide hepcidin is regulated by anemia, hypoxia, and inflammation. J Clin Invest 2002;110:1037-1044.
46. Vokurka M, Krijt J, Sulc K, Necas E. Hepcidin mRNA levels in mouse liver respond to inhibition of erythropoiesis. Physiol Res 2006;55:667-674.
47. Hunter HN, Fulton DB, Ganz T, Vogel HJ. The solution structure of human hepcidin, a peptide hormone with antimicrobial activity that is involved in iron uptake and hereditary hemochromatosis. J Biol Chem 2002;277:37597-37603.

48. Valore EV, Ganz T. Posttranslational processing of hepcidin in human hepatocytes is mediated by the prohormone convertase furin. Blood Cells Mol Dis 2008;40:132-138.
49. Nemeth E, Tuttle MS, Powelson J et al. Hepcidin regulates cellular iron efflux by binding to ferroportin and inducing its internalization. Science 2004;306:2090-2093.
50. Qiao B, Sugianto P, Fung E et al. Hepcidin-induced endocytosis of ferroportin is dependent on ferroportin ubiquitination. Cell Metab 2012;15:918-924.
51. Schmidt PJ, Toran PT, Giannetti AM et al. The transferring receptor modulates Hfe-dependent regulation of hepcidin expression. Cell Metab 2008;7:205-214.
52. Nemeth E, Rivera S, Gabayan V et al. IL-6 mediates hypoferremia of inflammation by inducing the synthesis of the iron regulatory hormone hepcidin. J Clin Invest 2004;113:1271-1276.
53. Bogdan AR, Miyazawa M, Hashimoto K, Tsuji Y. Regulators of iron homeostasis: new players in metabolism, cell death, and disease. Trends Biochem Sci 2016;41(3):274-286.
54. Zhang AS, Gao J, Koeberl DD, Enns CA. The role of hepatocyte hemojuvelin in the regulation of bone morphogenic protein-6 and hepcidin expression in vivo. J Biol Chem 2010;285:16416-16423.
55. Xia Y, Babitt JL, Sidis Y et al. Hemojuvelin regulates hepcidin expression via a selective subset of BMP ligands and receptors independently of neogenin. Blood 2008;111:5195-5204.
56. Babitt JL, Huang FW, Wrighting DM et al. Bone morphogenetic protein signaling by hemojuvelin regulates hepcidin expression. Nat Genet 2006;38:531-539.
57. Truksa J, Peng H, Lee P, Beutler E. Bone morphogenetic proteins 2, 4, and 9 stimulate murine hepcidin 1 expression independently of Hfe, transferrin receptor 2 (Tfr2), and IL-6. Proc Natl Acad Sci USA 2006;103:10289-10293.

58. Truksa J, Lee P, Beutler E. Two BMP responsive elements, STAT, and bZIP/HNF4/COUP motifs of the hepcidin promoter are critical for BMP, SMAD1, and HJV responsiveness. Blood 2009;113:688-695.
59. Casanovas G, Mleczko-Sanecka K, Altamura S et al. Bone morphogenetic protein (BMP)-responsive elements located in the proximal and distal hepcidin promoter are critical for its response to HJV/BMP/SMAD. J Mol Med (Berl) 2009;87:471-480.
60. Gross CN, Irrinki A, Feder JN, Enns CA. Co-trafficking of HFE, a nonclassical major histocompatibility complex class I protein, with the transferrin receptor implies a role in intracellular iron regulation. J Biol Chem 1998;273:22068-22074.
61. Gao J, Chen J, Kramer M et al. Interaction of the hereditary hemochromatosis protein HFE with transferrin receptor 2 is required for transferrin-induced hepcidin expression. Cell Metab 2009;9:217-227.
62. Ramey G, Deschemin JC, Vaulont S. Cross-talk between the mitogen activated protein kinase and bone morphogenetic protein/hemojuvelin pathways is required for the induction of hepcidin by holotransferrin in primary mouse hepatocytes. Haematologica 2009;94:765-772.
63. Ganz T, Nemeth E. Iron homeostasis in host defence and inflammation. Nat Rev Immunol 2015;15(8):500-510.
64. Nemeth E, Valore EV, Territo M et al. Hepcidin, a putative mediator of anemia of inflammation, is a type II acute-phase protein. Blood 2003;101:2461-2463.
65. Lee P., Peng H., Gelbart T et al. Regulation of hepcidin transcription by interleukin-1 and interleukin-6. Proc Natl Acad Sci USA 2005;102:1906-1910.
66. Inamura K, Matsuzaki Y, Uematsu N et al. Rapid inhibition of MAPK signaling and anti-proliferation effect via JAK/STAT signaling by interferon-alpha in hepatocellular carcinoma cell lines. Biochim Biophys Acta 2005;1745:401-410.

67. Wrighting DM, Andrews NC. Interleukin-6 induces hepcidin expression through STAT3. Blood 2006;108:3204-3209.
68. Canonne-Hergaux F, Gruenheid S, Govoni G, Gros P. The Nramp1 protein and its role in resistance to infection and macrophage function. Proc Assoc Am Physicians 1999;111:283-289.
69. Haase VH. Hypoxic regulation of erythropoiesis and ironmetabolism. Am J Physiol Renal Physiol 2010;299:F1-F13.
70. Lok CN, Ponka P. Identification of a hypoxia response element in the transferring receptor gene. J Biol Chem 1999;274:24147-24152.
71. Mukhopadhyay CK, Mazumder B, Fox PL. Role of hypoxia-inducible factor-1 in transcriptional activation of ceruloplasmin by iron deficiency. J Biol Chem 2000;275:21048-21054.
72. Shah YM, Matsubara T, Ito S et al. Intestinal hypoxia-inducible transcription factors are essential for iron absorption following iron deficiency. Cell Metab 2009;9:152-164.
73. Lee PJ, Jiang BH, Chin BY et al. Hypoxiainducible factor-1 mediates transcriptional activation of the heme oxygenase-1 gene in response to hypoxia. J Biol Chem 1997;272:5375-5381.
74. Jacobson LO, Goldwasser E, Fried W, Plzak LF. Studies on erythropoiesis. VII. The role of the kidney in the production of erythropoietin. Trans Assoc Am Phys 1957;70:305-317.
75. Andrews NC. Disorders of iron metabolism. N Engl J Med 1999;341:1986-1995.
76. Deugnier Y, Turlin B. Pathology of hepatic iron overload. World J Gastroenterol 2007;13:4755-4760.
77. Clark SF. Iron deficiency anemia. Nutr Clin Pract 2008;23:128-141.
78. Weiss G, Goodnough LT. Anemia of chronic disease. N Engl J Med 2005;352:1011-1023.
79. Beutler E. Iron storage disease: facts, fiction and progress. Blood Cells Mol Dis 2007;39:140-147.

80. Pietrangelo A. Hereditary hemochromatosis: pathogenesis, diagnosis, and treatment. Gastroenterology 2010;139:393-408.
81. Feder JN, Gnirke A, Thomas W et al. A novel MHC class I-like gene is mutated in patients with hereditary haemochromatosis. Nat Genet 1996;13:399-408.
82. Roetto A, Papanikolaou G, Politou M et al. Mutant antimicrobial peptide hepcidin is associated with severe juvenile hemochromatosis. Nat Genet 2003;33:21-22.
83. Papanikolaou G, Samuels ME, Ludwig EH et al. Mutations in HFE2 cause iron overload in chromosome 1q-linked juvenile hemochromatosis. Nat Genet 2004;36:77-82.
84. Sham RL, Phatak PD, West C et al. Autosomal dominant hereditary hemochromatosis associated with a novel ferroportin mutation and unique clinical features. Blood Cells Mol Dis 2005;34:157-161.
85. Camaschella C, Roetto A, Cali A et al. The gene TFR2 is mutated in a new type of haemochromatosis mapping to 7q22. Nat Genet 2000;25:14-15.
86. Feder JN, Tsuchihashi Z, Irrinki A et al. The hemochromatosis founder mutation in HLA-H disrupts beta2-microglobulin interaction and cell surface expression. J Biol Chem 1997;272:14025-14028.
87. Kono S. Aceruloplasminemia: an update. Int Rev Neurobiol 2013;110:125-151.
88. Aslan D, Crain K, Beutler E. A new case of human atransferrinemia with a previously undescribed mutation in the transferrin gene. Acta Haematol 2007;118:244-247.
89. Beghe C, Wilson A, Ershler WB. Prevalence and outcomes of anemia in geriatrics: a systematic review of the literature. Am J Med 2004;116 (Suppl 7A):3S–10S.
90. Merryweather-Clarke AT, Pointon JJ, Shearman JD, Robson KJ. Global prevalence of putative haemochromatosis mutations. J Med Genet 1997;34:275-278.

91. Hartman KR, Barker JA. Microcytic anemia with iron malabsorption: an inherited disorder of iron metabolism. Am J Hematol 1996;51:269-275.
92. Finberg KE, Heeney MM, Campagna DR et al. Mutations in TMPRSS6 cause iron-refractory iron deficiency anemia (IRIDA). Nat Genet 2008;40:569-571.
93. Yoshioka Y, Kosaka N, Ochiya T, Kato T. Micromanaging iron homeostasis: hypoxia-inducible micro-RNA-210 suppresses iron homeostasis-related proteins. J Biol Chem 2012;287:34110-34119.
94. Müller-Taubenberger A, Kortholt A, Eichinger L. Simple system--substantial share: the use of Dictyostelium in cell biology and molecular medicine. Eur J Cell Biol 2013;92(2):45-53.
95. Eichinger, L, Pachebat JA, Glöckner G et al. The genome of the social amoeba Dictyostelium discoideum. Nature 2005;435:43-57.
96. Bozzaro S, Eichinger L. The professional phagocyte Dictyostelium discoideum as a model host for bacterial pathogens. Curr Drug Targets 2011;12(7):942-954.
97. van Driessche N, Shaw C, Katoh M et al. A transcriptional profile of multicellular development in Dictyostelium discoideum. Development 2002;129:1543-1552.
98. Aderem A, Underhill DM. Mechanisms of phagocytosis in macrophages. Annu Rev Immunol 1999;17:593-623.
99. Jin T, Xu X, Fang J et al. How human leukocytes track down and destroy pathogens: lessons learned from the model organism Dictyostelium discoideum. Immunol Res 2009;43(1-3):118-127.
100. May RC, Machesky LM. Plagiarism and pathogenesis: common themes in actin remodeling. Dev Cell 2001;1:317-318.
101. Devreotes PN, Zigmond SH. Chemotaxis in eukaryotic cells: a focus on leukocytes and Dictyostelium. Annu Rev Cell Biol 1988;4:649-686.
102. Thilo L. Quantification of endocytosis-derived membrane traffic. Biochim Biophys Acta 1985;822:243-266.

103. Peracino B, Borleis J, Jin T et al. G-protein beta subunit-null mutants are impaired in phagocytosis and chemotaxis due to inappropriate regulation of the actin cytoskeleton. J Cell Biol 1998;141:1529-1537.
104. Rosenberger CM, Finlay BB. Phagocyte sabotage: disruption of macrophage signalling by bacterial pathogens. Nat Rev Mol Cell Biol 2003;4:385-396.
105. Garin J, Diez R, Kieffer S et al. The phagosome proteome: insight into phagosome functions. J Cell Biol 2001;152:165-180.
106. Cardelli J. Phagocytosis and macropinocytosis in Dictyostelium: phosphoinositide-based processes, biochemically distinct. Traffic 2001;2:311-320.
107. Cosson P, Soldati T. Eat, kill or die: when amoeba meets bacteria. Curr Opin Microbiol 2008;11:271-276.
108. Bozzaro S, Buracco S, Peracino B. Iron metabolism and resistance to infection by invasive bacteria in the social amoeba Dictyostelium discoideum. Front Cell Infect Microbiol 2013;19(3):1-9.
109. Bozzaro S, Bucci C, Steinert M. Phagocytosis and host-pathogen interactions in Dictyostelium with a look at macrophages. Int Rev Cell Mol Biol 2008;271:253-300.
110. Dorer MS, Isberg RR. Non-vertebrate hosts in the analysis of host pathogen interactions. Microbes Infect 2006;8:1637-1646.
111. Haas A. The phagosome: compartment with a license to kill. Traffic 2007;8(4):311-330.
112. Rupper A, Grove B, Cardelli J. Rab7 regulates phagosome maturation in Dictyostelium. J Cell Sci 2001;114:2449-2460.
113. Gotthardt D, Warnatz HJ, Henschel O et al. High-resolution dissection of phagosome maturation reveals distinct membrane trafficking phases. Mol Biol Cell 2002;13:3508-3520.
114. Clarke M, Kohler J, Arana Q et al. Dynamics of the vacuolar H+-ATPase in the contractile vacuole complex and the endosomal pathway of Dictyostelium cells. J Cell Sci 2002;115:2893-2905.

115. Peracino B, Wagner C, Balest A, et al. Function and mechanism of action of Dictyostelium Nramp1 (Slc11a1) in bacterial infection. Traffic 2006;7(1):22-38.
116. Peracino B, Balest A, and Bozzaro S. Phosphoinositides differentially regulate bacterial uptake and Nramp1-induced resistance to Legionella infection in Dictyostelium. J Cell Sci 2010;123:4039-4051.
117. Francione L, Smith PK, Accari SL et al. Legionella pneumophila multiplication is enhanced by chronic AMPK signalling in mitochondrially diseased Dictyostelium cells. Dis Model Mech 2009;2:479-489.
118. Hagedorn M, Rohde KH, Russell DG, and Soldati T. Infection by tubercular mycobacteria is spread by nonlytic ejection from their amoeba hosts. Science 2009;323:1729-1733.
119. Parra-Lopez C, Lin R, Aspedon A, Groisman EA. A Salmonella protein that is required for resistance to antimicrobial peptides and transport of potassium. EMBO J 1994;13(17):3964-3972.
120. Blanc-Potard AB, Groisman EA. The Salmonella selC locus contains a pathogenicity island mediating intramacrophage survival. EMBO J 1997;16(17):5376-5385.
121. Ammendola S, Pasquali P, Pistoia C, et al. High-affinity Zn^{2+} uptake system ZnuABC is required for bacterial zinc homeostasis in intracellular environments and contributes to the virulence of Salmonella enterica. Infect Immun 2007;75(12):5867-5876.
122. Papp-Wallace KM, Nartea M, Kehres DG, et al. The CorA Mg^{2+} channel is required for the virulence of Salmonella enterica serovar typhimurium. J Bacteriol 2008;190(19):6517-6523.
123. Gobin J, Horwitz MA. Exochelins of Mycobacterium tuberculosis remove iron from human iron-binding proteins and donate iron to mycobactins in the M. tuberculosis cell wall. J Exp Med 1996;183(4):1527-1532.
124. Robey M, Cianciotto NP. Legionella pneumophila feoAB promotes ferrous iron uptake and intracellular infection. Infect Immun 2002;70(10):5659-5669.

125. De Voss JJ, Rutter K, Schroeder BG et al. The salicylate-derived mycobactin siderophores of Mycobacterium tuberculosis are essential for growth in macrophages. Proc Natl Acad Sci USA 2000;97(3):1252-1257.
126. Courville P, Chaloupka R, Cellier MF. Recent progress in structure-function analyses of Nramp proton-dependent metal-ion transporters. Biochem Cell Biol 2006;84(6):960-978.
127. Bellamy R. Susceptibility to mycobacterial infections: the importance of host genetics. Genes Immun 2003;4(1):4-11.
128. Jabado N, Cuellar-Mata P, Grinstein S, Gros P. Iron chelators modulate the fusogenic properties of Salmonella-containing phagosomes. Proc Natl Acad Sci USA 2003;100(10):6127-6132.
129. Malik S, Abel L, Tooker H et al. Alleles of the NRAMP1 gene are risk factors for pediatric tuberculosis disease. Proc Natl Acad Sci USA 2005;102(34):12183-12188.
130. Vidal SM, Pinner E, Lepage P et al. Natural resistance to intracellular infections: Nramp1 encodes a membrane phosphoglycoprotein absent in macrophages from susceptible (Nramp1, D169) mouse strains. J Immunol 1996;157:3559-3568.
131. Forbes JR, Gros P. Divalent-metal transport by NRAMP proteins at the interface of host–pathogen interactions. Trends Microbiol 2001;9:397-403.
132. Shawki A, Knight P, Maliken B et al. H(+)-coupled divalent metal-ion transporter-1: functional properties, physiological role and therapeutics. Curr Top Membr 2012;70:169-214.
133. Nevo Y, and Nelson N. The NRAMP family of metal-ion transporters. Biochim Biophys Acta 2006;1763:609-620.
134. Papp-Wallace K, and Maguire M. Manganese transport and the role of manganese in virulence. Annu Rev Microbiol 2006;60:187-209.
135. Cellier M. Nutritional immunity: homology modeling of Nramp metal import. Adv Exp Med Biol 2012;946:335-351.

136. Heuser J, Zhu QL, and Clarke M. Proton pumps populate the contractile vacuoles of Dictyostelium amoebae. J Cell Biol 1993;121:1311-1327.
137. Clarke M, Kohler J, Arana Q et al. Dynamics of the vacuolar H^+-ATPase in the contractile vacuole complex and the endosomal pathway of Dictyostelium cells. J Cell Sci 2002;115:2893-2905.
138. Richer E, Courville P, Bergevin I and Cellier MFM. Horizontal gene transfer of "prototype" Nramp in bacteria. J Mol Evol 2003;57:363-376.
139. Ehrnstorfer IA, Geertsma ER, Pardon E et al. Crystal structure of a SLC11 (NRAMP) transporter reveals the basis for transition-metal ion transport. Nat Struct Mol Biol 2014;21(11):990-996.
140. Cohen A, Nelson H and Nelson N. The family of SMF metal ion transporters in Yeast cells. J Biol Chem 2000;275:33388-33394.
141. Portnoy ME, Liu XF and Culotta VC. Saccharomyces cerevisiae expresses three functionally distinct homologues of the Nramp family of metal transporters. Mol Cell Biol 2000;20:7893-7902.
142. Lin L, Yee SW, Kim RB, Giacomini KM. SLC transporters as therapeutic targets: emerging opportunities. Nat Rev Drug Discov 2015;14(8):543-560.
143. Hediger MA, Clémençon B, Burrier RE, Bruford EA. The ABCs of membrane transporters in health and disease (SLC series): introduction. Mol Aspects Med 2013;34(2-3):95-107.
144. Borst P, Elferink RO. Mammalian ABC transporters in health and disease. Annu Rev Biochem 2002;71:537-592.
145. Cox DW, Moore SD. Copper transporting P-type ATPases and human disease. J Bioenerg Biomembr 2002;34(5):333-338.
146. Dunbar LA, Caplan MJ. The cell biology of ion pumps: sorting and regulation. Eur J Cell Biol 2000;79(8):557-563.
147. Muller V, Gruber G. ATP synthases: structure, function and evolution of unique energy converters. Cell Mol Life Sci 2003;60(3):474-494.
148. Armstrong CM. Voltage-gated K channels. Sci 2003;STKE:re10.

149. Decoursey TE. Voltage-gated proton channels and other proton transfer pathways. Physiol Rev 2003;83(2):475-579.
150. Jiang Y, Ruta V, Chen J et al. The principle of gating charge movement in a voltage-dependent K+ channel. Nature 2003;423(6935):42-48.
151. Yu FH, Catterall WA. Overview of the voltage-gated sodium channel family. Genome Biol 2003;4(3):207.
152. César-Razquin A, Snijder B, Frappier-Brinton T et al. A call for systematic research on solute carriers. Cell 2015;162(3):478-487.
153. Nigam SK. What do drug transporters really do? Nat Rev Drug Discov 2015;14:29-44.
154. Sai Y. Biochemical and molecular pharmacological aspects of transporters as determinants of drug disposition. Drug Metab Pharmacokinet 2005;20(2):91-99.
155. Hediger MA, Romero MF, Peng JB et al. The ABCs of solute carriers: physiological, pathological and therapeutic implications of human membrane transport proteins. Pflugers Arch 2004;447:465-468.
156. Penmatsa A, Wang KH and Gouaux E. X-ray structure of dopamine transporter elucidates antidepressant mechanism. Nature 2013;503:85-90.
157. Newstead S, Drew D, Cameron AD et al. Crystal structure of a prokaryotic homologue of the mammalian oligopeptide-proton symporters, PepT1 and PepT2. EMBO J 2011;30:417-426.
158. Colas C, Ung PM, Schlessinger A. SLC transporters: structure, function, and drug discovery. Med chem commun 2016;7(6):1069-1081.
159. Radestock S and Forrest LR. The alternating-access mechanism of MFS transporters arises from inverted-topology repeats. J Mol Biol 2011;407:698-715.
160. Kaback HR, Smirnova I, Kasho V et al. The alternating access transport mechanism in LacY. J Membr Biol 2011;239:85-93.
161. Forrest LR and Rudnick G. The rocking bundle: a mechanism for ion-coupled solute flux by symmetrical transporters. Physiology 2009;24:377-386.

162. Yamashita A, Singh SK, Kawate T et al. Crystal structure of a bacterial homologue of Na^+/Cl^--dependent neurotransmitter transporters. Nature 2005;437:215-223.
163. Singh SK and Pal A. Biophysical approaches to the study of LeuT, a prokaryotic homolog of neurotransmitter sodium symporters. Methods Enzymol 2015;557:167-198.
164. Penmatsa A and Gouaux E. How LeuT shapes our understanding of the mechanisms of sodium-coupled neurotransmitter transporters. J Physiol 2014; 592:863-869.
165. Reyes N, Ginter C and Boudker O. Transport mechanism of a bacterial homologue of glutamate transporters. Nature 2009;462:880-885.
166. Verdon G and Boudker O. Crystal structure of an asymmetric trimer of a bacterial glutamate transporter homolog. Nat Struct Mol Biol 2012;19:355-357.
167. Yernool D, Boudker O, Jin Y and Gouaux E. Structure of a glutamate transporter homologue from Pyrococcus horikoshii. Nature 2004;431:811-818.
168. Williams AL, Jacobs SB, Moreno-Macias H et al. Sequence variants in SLC16A11 are a common risk factor for type 2 diabetes in Mexico. Nature 2014;506:97-101.
169. Montalbetti N, Simonin A, Kovacs G & Hediger MA. Mammalian iron transporters: families SLC11 and SLC40. Mol Aspects Med 2013;34:270-287.
170. Cellier MF, Bergevin I, Boyer E & Richer E. Polyphyletic origins of bacterial Nramp transporters. Trends Genet 2001;17:365-370.
171. Bozzi AT, Bane LB, Weihofen WA et al.Conserved methionine dictates substrate preference in Nramp-family divalent metal transporters. Proc Natl Acad Sci USA 2016;113(37):10310-10315.
172. Gruenheid S, Pinner E, Desjardins M, Gros P. Natural resistance to infection with intracellular pathogens: the Nramp1 protein is recruited to the membrane of the phagosome. J Exp Med 1997;185(4):717-730.

173. Vidal SM, Malo D, Vogan K et al. Natural resistance to infection with intracellular parasites: isolation of a candidate for Bcg. Cell 1993;73:469-485.
174. Cellier MF, Courville P, Campion C. Nramp1 phagocyte intracellular metal withdrawal defense. Microbes Infect 2007;9(14-15):1662-1670.
175. Gruenheid S, Canonne-Hergaux F, Gauthier S et al. The iron transport protein NRAMP2 is an integral membrane glycoprotein that colocalizes with transferrin in recycling endosomes. J Exp Med 1999;189(5):831-841.
176. Lee PL, Gelbart T, West C et al. The human Nramp2 gene: characterization of the gene structure, alternative splicing, promoter region and polymorphisms. Blood Cells Mol Dis 1998;24:199-215.
177. Canonne-Hergaux F, Gros P. Expression of the iron transporter DMT1 in kidney from normal and anemic mk mice. Kidney Int 2002;62(1):147-156.
178. Fleming MD,. Trenor III CC, Su MA et al. Microcytic anaemia mice have a mutation in Nramp2, a candidate iron transporter gene. Nat Genet 1997;16:383-386.
179. Shawki A & Mackenzie B. Interaction of calcium with the human divalent metal-ion transporter-1. Biochem Biophys Res Commun 2010;393:471-475.
180. Mackenzie B, Ujwal ML, Chang MH et al. Divalent metal-ion transporter DMT1 mediates both H^+ -coupled Fe^{2+} transport and uncoupled fluxes. Pflugers Arch 2006;451:544-558.
181. Lam-Yuk-Tseung S, Govoni G, Forbes J & Gros P. Iron transport by Nramp2/DMT1: pH regulation of transport by 2 histidines in transmembrane domain 6. Blood 2003;101:3699-3707.
182. Nevo Y, Nelson N. The mutation F227I increases the coupling of metal ion transport in DCT1. J Biol Chem 2004;279(51):53056-53061.
183. Nevo Y. Site-directed mutagenesis investigation of coupling properties of metal ion transport by DCT1. Biochim Biophys Acta 2008;1778(1):334-341.
184. Peracino B, Buracco S and Bozzaro S. The Nramp (Slc11) proteins regulate development, resistance to pathogenic bacteria and iron homeostasis in Dictyostelium discoideum. J Cell Sci 2013;126:301-311.

185. Cohen A, Nevo Y and Nelson H. The first external loop of the metal ion transporter DCT1 is involved in metal ion binding and specificity. Proc Natl Acad Sci USA 2003;100:10694-10699.
186. Marciani P, Trotti D, Hediger MA, Monticelli G. Modulation of DMT1 activity by redox compounds. J Membr Biol 2004;197(2):91-99.
187. Sacher A, Cohen A and Nelson N. Properties of the mammalian and yeast metal-ion transporters DCT1 and Smf1p expressed in Xenopus laevis oocytes. J Exp Biol 2001;204:1053-1061.
188. Chen XZ, Peng JB, Cohen A et al. Yeast SMF1 mediates H^+-coupled iron uptake with concomitant uncoupled cation currents. J Biol Chem 1999;274:35089-35094.
189. Nelson N, Sacher A and Nelson H. The significance of molecular Slips in transport systems. Nat Rev Mol Cell Biol 2002;3:876-881.
190. Hille B. Ion channels of excitable membranes. Chapter 10:309-345. Sinauer Inc. 3rd ed.
191. Czachorowski M, Lam-Yuk-Tseung S, Cellier M and Gros P. Transmembrane topology of the mammalian Slc11a2 iron transporter. Biochemistry 2009;48:8422-8434.
192. Illing A, Shawki A, Cunningham CL and Mackenzie B. Substrate profile and metal-ion selectivity of human divalent metal-ion transporter-1. J Biol Chem 2012;287:30485-30496.
193. Buracco S, Peracino B, Cinquetti R et al. Dictyostelium Nramp1, which is structurally and functionally similar to mammalian DMT1 transporter, mediates phagosomal iron efflux. J Cell Sci 2015;128(17):3304-3316.

Che dire……sono felice di tutto il periodo passato all'Insubria, specialmente per le persone veramente speciali che ci sono sempre state in questi anni…..visto che ai 3 canonici ho pensato bene di aggiungerci quasi un anno per avere Carlotta tra voi!

Grazie alla Prof. Bossi, ovvero Elena, per avermi accolto in laboratorio nonostante fossi completamente digiuna di tecniche elettrofisiologiche…..mi ricordo ancora la frase dopo aver visitato la stanza coi Voltage……"Ah di tutti questi macchinari in lab riconosco solo la bilancia…..", ora mi sento arricchita e me ne vado sicura di avere acquisito tanto e con sicurezza.
Grazie alla mia famiglia, tanto travagliata in questo periodo, ma che mi ha sempre sostenuto nelle mie scelte, mi ha permesso di fare sempre quello che più mi piaceva, in silenzio, senza chiedere molto, anche perchè parlare di scienza in genere non è facile!

Grazie alle Dottorande che mi hanno accolto nell'ormai lontano febbraio 2013, Alessandra ed Eleonora. All'inizio la differenza anagrafica mi ha fatto fare fatica…..interagire con persone così giovani, conquistare la loro fiducia è stata dura, ma alla fine siamo riuscite a diventare un tuttuno, noi, la rana, le iniezioni del venerdì e le serate al voltage fino all'ultimo oocita!!!

Alessandra poi nel secondo periodo di dottorato è stata la mia compagna, il lavoro sui D-aa è il nostro bambino su cui abbiamo lavorato e riso gomito a gomito…..e poi l'arrivo delle chimere, la creazione delle quali mi ha impegnato non poco…..e sulle quali abbiamo sudato entrambe!

Sudato anche più del dovuto visto che per un periodo abbiamo dovuto fare a meno della super Raffy (Benvenuto Ale!!!)…..che dire di te, sei stata dal mio ritorno post-Carlotta la persona su cui fare affidamento SEMPRE, al 100%, sia per la scienza che per il resto della vita, visto che noi "cinesine" in comune abbiamo tanto……non solo l'abito delle spose di Gio, almeno lo spero perchè sei veramente una bella persona e ti voglio bene, lo sai anche se non te lo dico mai!!!

Non posso poi dimenticare SaraHH, senza di te sarei stata ancora lì a fare intestazioni imprecando non poco…..GRAZIEEEEEE!!!!!

Paola Campo, mi mancherà la tua super risata, sei sempre positiva e sei una persona che non s'abbatte mai, mi hai sempre aiutato e chiarito ogni aspetto genetico nebuloso che ti ho sottoposto, grazie!

Le PIRNE….sono sempre stata bene con voi a meno che non sbattessi le porte……..spero di cavarmela così e non dover anche pagare pegno a Betta per le consulenze informatiche……Grazie anche a voi per il cammino parallelo al mio, nel lab di fianco!!

Non posso nemmeno dimenticare ROSS, senza di te non avrei avuto le foto delle immuno…….preziosa più che mai e sempre disponibile….GRAZIE!!

Non posso dimenticare i "nuovi" dottorandi che insieme a me lavorano tutt'oggi, Daniele e Francesca, grazie di cuore anche a voi e ai numerosi tesisti passati in laboratorio, Deb Tond e Martina nel cuore!!

In ultimo non posso dimenticare chi c'è sempre stato e sempre ci sarà…..almeno spero! Adry è la seconda discussione di tesi che ascolti, la prima era pure coi lucidi nel lontano Giurassico; spero di essere la tua persona sempre, anche se so bene che è dura sopportarmi tutti i giorni. Cerca di condividere con me questo momento e cerca di apprezzarmi anche come Dottore di Ricerca in Fisiologia Sperimentale e Clinica….visto che questo ho cercato di fare negli ultimi 4 anni, in silenzio, senza raccontare troppo…..ma felice per quello che ho fatto, sempre!